Redox Biology 20 (2019) 46–59

Contents lists available at ScienceDirect

Redox Biology

journal homepage: www.elsevier.com/locate/redox

Homocysteine causes vascular endothelial dysfunction by disrupting endoplasmic reticulum redox homeostasis

Xun Wu[a,b], Lihui Zhang[a,b], Yütong Miao[c], Juan Yang[c], Xian Wang[c], Chih-chen Wang[a,b], Juan Feng[c,*], Lei Wang[a,b,**]

[a] National Laboratory of Biomacromolecules, CAS Center for Excellence in Biomacromolecules, Institute of Biophysics, Chinese Academy of Sciences, Beijing 100101, China

[b] College of Life Sciences, University of Chinese Academy of Sciences, Beijing 100049, China

[c] Department of Physiology and Pathophysiology, School of Basic Medical Sciences, Peking University Health Science Center, Key Laboratory of Molecular Cardiovascular Science, Ministry of Education, Beijing 100191, China

ARTICLE INFO

Keywords:
Endothelial cells
Endoplasmic reticulum
Ero1α
GPx7
Homocysteine
Redox homeostasis

ABSTRACT

Endothelial dysfunction induced by hyperhomocysteinemia (HHcy) plays a critical role in vascular pathology. However, little is known about the role of endoplasmic reticulum (ER) redox homeostasis in HHcy-induced endothelial dysfunction. Here, we show that Hcy induces ER oxidoreductin-1α (Ero1α) expression with ER stress and inflammation in human umbilical vein endothelial cells and in the arteries of HHcy mice. Hcy upregulates Ero1α expression by promoting binding of hypoxia-inducible factor 1α to the *ERO1A* promoter. Notably, Hcy rather than other thiol agents markedly increases the GSH/GSSG ratio in the ER, therefore allosterically activating Ero1α to produce H_2O_2 and trigger ER oxidative stress. By contrast, the antioxidant pathway mediated by ER glutathione peroxidase 7 (GPx7) is downregulated in HHcy mice. Ero1α knockdown and GPx7 overexpression protect the endothelium from HHcy-induced ER oxidative stress and inflammation. Our work suggests that targeting ER redox homeostasis could be used as an intervention for HHcy-related vascular diseases.

1. Introduction

Hyperhomocysteinemia (HHcy) has been recognized as an independent risk factor for cardiovascular diseases [1–4]. Endothelial dysfunction induced by HHcy plays a critical role in vascular pathology, and accumulating data suggest that cellular oxidative stress [5] and endoplasmic reticulum (ER) stress lead to endothelial dysfunction [6], inflammation and atherosclerosis [7,8]. However, the mechanism by which Hcy induces endothelial ER stress and oxidative stress is still poorly understood. Particularly, little is known about the role of ER redox homeostasis in HHcy-induced endothelial dysfunction.

Multiple effects of homocysteine (Hcy) are due to the high reactivity of its sulfhydryl group. We have reported that reactive oxygen species (ROS) generated by thiol (–SH) auto-oxidation of Hcy are essential in Hcy-induced B lymphocyte proliferation and susceptibility to inflammatory progression of atherosclerotic lesions [9]. In endothelial cells, Hcy has also been reported to induce ROS production by NADPH oxidases [10,11] and endothelial NO synthase uncoupling [12,13]. Elevated ROS levels result in protein and DNA damage, further leading to inflammation and cell death [14]. Moreover, increasing Hcy concentration elicits ER stress and activates the unfolded protein response (UPR). Prolonged UPR activity may lead to ER stress-induced cell death [15].

The ER is the compartment for the folding and assembly of secretory and membrane proteins, many of which (e.g., cytokines, immunoglobulins and receptors) are rich in disulfide bonds. The folding of proteins containing disulfide bonds, also known as oxidative protein folding, is catalyzed by a series of enzymes in the ER lumen [16]. The ER sulfhydryl oxidase Ero1α catalyzes *de novo* disulfide bond formation by transferring electrons to molecular oxygen, generating equimolar disulfide and hydrogen peroxide (H_2O_2) [17]. The disulfide is then transferred to the active site of protein disulfide isomerase (PDI) and, in turn, to the nascent peptides [17,18]. It is estimated that Ero1α-mediated disulfide formation can account for up to 25% of cellular peroxide/superoxide produced during protein synthesis, while the other 75% come from ATP production through respiration [17]. Although H_2O_2

* Corresponding author.
** Corresponding author at: National Laboratory of Biomacromolecules, CAS Center for Excellence in Biomacromolecules, Institute of Biophysics, Chinese Academy of Sciences, Beijing 100101, China.
E-mail addresses: juanfeng@bjmu.edu.cn (J. Feng), wanglei@moon.ibp.ac.cn (L. Wang).

https://doi.org/10.1016/j.redox.2018.09.021
Received 27 July 2018; Received in revised form 18 September 2018; Accepted 26 September 2018
Available online 26 September 2018

may function as a second messenger by chemoselective oxidation of cysteine residues, excess H_2O_2 can exert a toxic effect on cells by causing over-oxidation of proteins and DNA [19,20]. There is accumulating evidence that oxidative protein folding in the ER is a source of ER over-oxidation and stress [17,21,22], termed as ER oxidative stress. Thus, Ero1α activity must be tightly regulated in order to prevent excess ROS accumulation and ER oxidative stress. It has been known that the activity of Ero1α is feedback regulated by PDI and its homologues to maintain redox balance in the ER [23–25]. Interestingly, Hcy was reported to activate Ero1α in the gastrointestinal tract [26]; however, the underlying mechanism and pathological significance to cardiovascular disease are still unknown.

The glutathione peroxidase (GPx) family is a class of major antioxidant enzymes that catalyze the reduction of H_2O_2 [27]. The family comprises eight members, GPx1–GPx8, of which only GPx7 and GPx8 are located in the ER [28]. In HHcy mice, the regulation of GPx1 is directly linked to the endothelial function and vascular homeostasis [29]. We and others have showed that GPx7 and GPx8 can eliminate Ero1α-produced H_2O_2. Specifically, the Ero1α/GPx7/PDI triad couples H_2O_2 elimination and disulfide generation to ensure efficient and safe oxidative protein folding [30]. Interestingly, deficiency of GPx7 is associated with increased carcinogenesis and shortened lifespan [31,32]. Nevertheless, whether GPx7 plays a role and the relationship between GPx7 and Ero1α in Hcy-induced ER oxidative stress are still open questions.

Here, we reported that Hcy induced the expression of ER sulfhydryl oxidase Ero1α, together with ER stress and inflammation, in human umbilical vein endothelial cells (HUVECs) and in the arteries of HHcy mice. At the transcriptional level, Hcy promoted the binding of hypoxia-inducible factor 1α (HIF-1α) to the promoter of *ERO1A* and upregulated Ero1α expression. At the post-translational level, Hcy allosterically activated Ero1α by increasing the GSH/GSSG ratio in the ER. The increased Ero1α activity produced excess H_2O_2 and led to protein over-oxidation in the ER, activation of the unfolded protein response (UPR) and endothelial inflammation. Knockdown of Ero1α ameliorated Hcy-induced ER oxidative stress and inflammation in endothelial cells both *in vivo* and *ex vivo*. On the other hand, the nuclear factor erythroid 2-related factor 2 (NRF2)-GPx7 antioxidant pathway was downregulated in HHcy mice. Overexpression of GPx7 protected the endothelium from Hcy-induced ER oxidative stress and inflammation in *in vivo* and *ex vivo* experiments. Altogether, HHcy disrupts the Ero1α/GPx7 balance and impairs ER redox homeostasis, leading to ER oxidative stress and endothelial inflammation.

2. Results

2.1. Ero1α expression is induced with ER stress and inflammation in the thoracic aortas of HHcy mice

Vascular ER stress and inflammation have been probed in chronic HHcy mice with a clinically relevant level of plasma Hcy (20–30 μM) [33]. Consistent with the previous study, we found that the IRE1 branch of the UPR was activated, manifested as an upregulated level of the spliced form of X-box-binding protein 1 (XBP1), in HHcy-treated mice compared with control mice (Fig. 1A). The PERK signaling pathway was also activated, increasing the level of phosphorylated eukaryotic initiation factor 2α (eIF2α), by HHcy stimulation (Fig. 1A). The adhesion molecules intercellular adhesion molecule-1 (ICAM-1) and vascular cell adhesion molecule-1 (VCAM-1) are two proinflammatory markers predominantly in vascular endothelium [34,35], which were significantly induced in HHcy mice (Fig. 1B). Since Hcy is a sulfur amino acid with reducing power, we next studied whether ER redox homeostasis could be affected by HHcy. As a pivotal ER sulfhydryl oxidase, Ero1α has been reported to be induced by reductive stress, such as hypoxia and DTT stimuli [26,36]. Interestingly, the expression of Ero1α was upregulated dramatically – approximately sixfold – in blood vessel of HHcy mice (Fig. 1B). Furthermore, as shown in Fig. 1C and D by immunofluorescence staining, increased expression of ICAM-1, VCAM-1, and Ero1α were found in thoracic aortas of HHcy mice. Altogether, these results suggest that Ero1α is elevated in the vasculature of an HHcy animal model and might be linked to Hcy-induced ER stress and vascular endothelial inflammation.

2.2. Hcy upregulates Ero1α and induces ER oxidative stress in HUVECs

Because endothelial dysfunction is regarded as a key early event in vascular disorders [37], we next explored the effects of Hcy on ER redox homeostasis in HUVECs. Hcy dose-dependently (100–1000 μM) upregulated the protein expression of Ero1α compared with PBS control (Fig. 2A). Meanwhile, BiP, the canonical ER stress marker, was also elevated by Hcy treatment, similar to the effects caused by the known ER stress inducer thapsigargin (Thaps, an inhibitor of SERCA calcium pump) (Fig. 2A). Actually, the free thiol (–SH) form of Hcy is involved in the pathological effects [38], and in HHcy mice the total Hcy is 25.28 μM and –SH form of Hcy is 0.58 μM [39,40]. For moderate HHcy administration (20–200 μM) *in vitro*, the concentration of –SH form of Hcy is determined to be around 0.2–2 μM [39], which is within the pathological range. Thus, for the following *in vitro* experiments, we typically used 200 μM Hcy, which has also been used in several studies to investigate the molecular and cellular mechanisms of HHcy [6,41]. We found that treating HUVECs with Hcy (200 μM) resulted in time-dependently (1–8 h) upregulation of Ero1α and BiP (Fig. 2B), similar to the pathological effects of chronic HHcy mice. In parallel, Hcy induced XBP-1 splicing and phosphorylation of eIF2α, indicating that an adaptive UPR was also triggered in HUVECs. Interestingly, the CHOP was induced at the late stage of Hcy treatment, implying that prolonged Hcy treatment may trigger fatal UPR.

Since Ero1α sulfhydryl oxidase catalyzes disulfide formation by utilizing molecular oxygen and produces H_2O_2. By using the Amplex red peroxide/peroxidase assay [42], which can be used to detect H_2O_2 at very low concentration (Fig. S1A), we monitored whether Hcy could induce H_2O_2 accumulation. Hcy dose-dependently (20–200 μM) increased H_2O_2 production in HUVECs (Fig. S1B). As shown in Fig. 2C, the effect of Hcy on H_2O_2 production is similar to dithiothreitol (DTT), a potent reducing agent and an artificial substrate of Ero1α [23,36]. More importantly, Hcy as low as 50 μM largely induced H_2O_2 accumulation; however, at this concentration other thiol agents including cysteine (Cys), N-acetylcysteine (NAC) and gluthathione (GSH) had little effect, indicating the specific effect of Hcy (Fig. 2C). The increase of H_2O_2 production by Hcy can be inhibited by an Ero1α inhibitor (EN460), but not by NOXs inhibitor (DPI) and eNOS inhibitor (L-NMMA) (Fig. 2D). One toxic effect of excess H_2O_2 is the oxidation of the cysteine residues in proteins, resulting in protein dysfunction. We then detected protein cysteine sulfenylation by using a dimedone-labelling method [20] in cells (Fig. 2E). As shown in Fig. 2F, sulfenylated proteins accumulated in 200 μM Hcy-treated HUVECs and largely co-localized with the ER lumen marker PDI. Therefore, Hcy effectively induces H_2O_2 accumulation in the ER of HUVECs, and Hcy-induced ER oxidative stress is likely through the upregulation of Ero1α.

2.3. HIF-1α mediates Hcy-induced Ero1α expression in HUVECs

It has been reported that HIF-1α, a proinflammatory transcription factor in endothelial dysfunction [43,44], can induce Ero1α during hypoxia [36,45]. We then hypothesized that HIF-1α is responsible for Hcy-induced expression of Ero1α. Indeed, there was an approximately fivefold increase in HIF-1α expression in the thoracic aortas of HHcy mice compared with control mice (Fig. 3A). In HUVECs, Hcy increased the expression of HIF-1α and its canonical downstream target, vascular endothelial growth factor (VEGF) (Fig. S2). Activation of HIF-1α by Hcy was confirmed by its nuclear accumulation; $CoCl_2$, a hypoxia-mimicking reagent for activating HIF-1α [46], also induced Ero1α

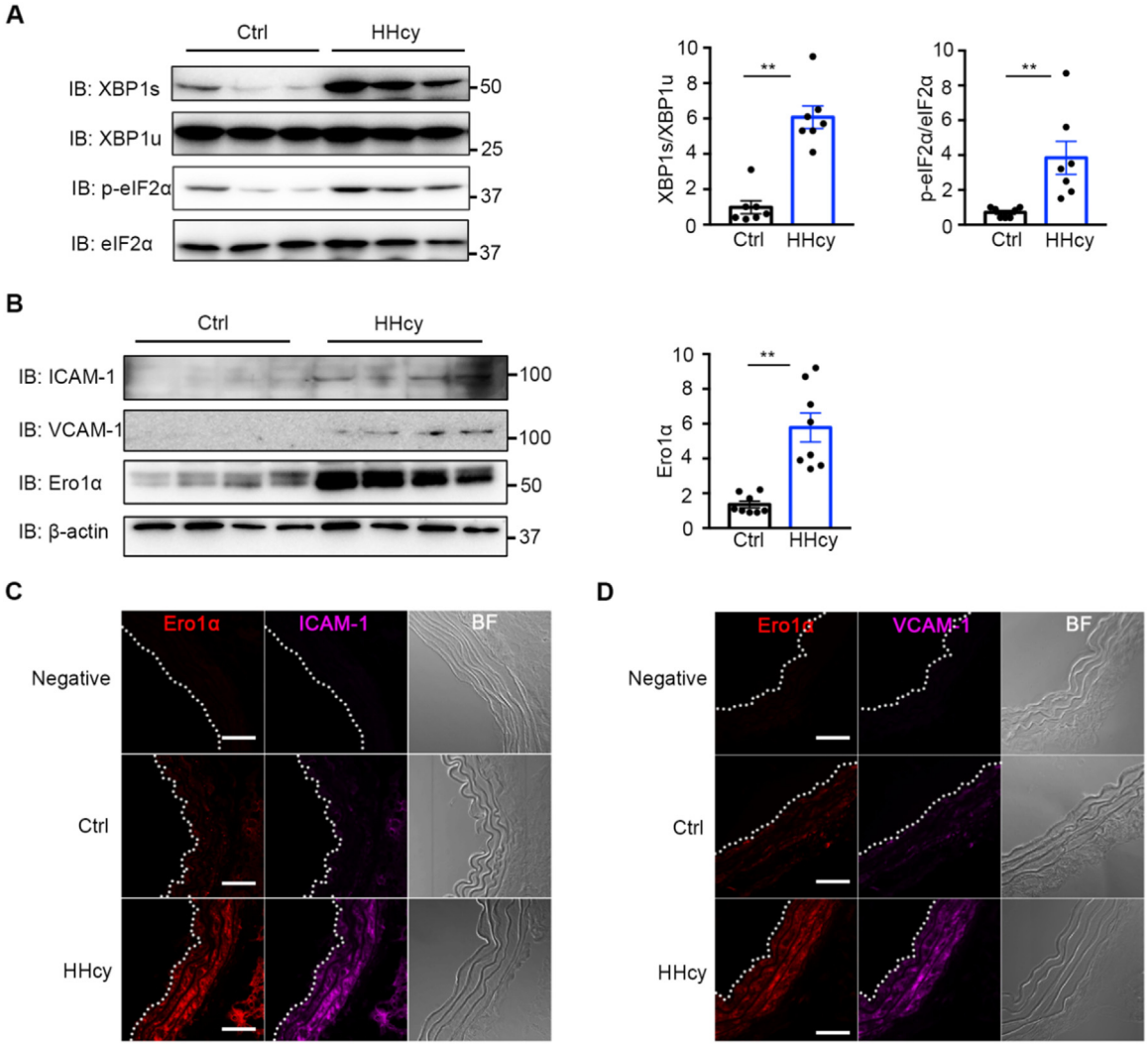

Fig. 1. Hcy induces ER stress and inflammation and upregulates Ero1α in the thoracic aortas of HHcy mice. (A) The lysates of the thoracic aortas in normal (Ctrl) and HHcy mice were subjected to immunoblotting analysis for spliced XBP1 (XBP1s), unspliced XBP1 (XBP1u), phosphorylated eIF2α (p-eIF2α), and eIF2α. Representative blots were shown. Statistical analysis for XBP1s/XBP1u and p-eIF2α/eIF2α was indicated. Data were presented as mean ± SEM from seven biological replicates, $^{**}p < 0.01$ *via* two-tailed Student's *t*-test. (B) Immunoblotting for expression of ICAM-1, VCAM-1, and Ero1α in the thoracic aortas of Ctrl and HHcy mice. Representative blots were shown. Statistical analysis for expression of Ero1α was indicated, normalized to β-actin. Data were presented as mean ± SEM from eight biological replicates, $^{**}p < 0.01$ *via* two-tailed Student's *t*-test. (C, D) Immunofluorescence analysis of Ero1α (red, Ex = 568 nm) and ICAM-1 (purple, Ex = 647 nm) (C) or VCAM-1 (purple, Ex = 647 nm) (D) in the thoracic aortas of Ctrl and HHcy mice. Immunofluorescence with rabbit Ig G was used as a negative control. The aortic intima is indicated by white dashed line. BF, bright field. Scale bars, 50 μm.

expression like Hcy (Fig. 3B). Acriflavine (ACF) can directly bind to HIF-1α and inhibit its DNA-binding and transcriptional activity [47]. We observed that ACF inhibited basal Ero1α expression in a dose-dependent manner (0.1–5 μM), accompanied by the accumulation of inactive HIF-1α in the nucleus (Fig. 3C). Moreover, ACF attenuated the Hcy-induced upregulation of Ero1α protein expression (Fig. 3D). In addition, depletion of HIF-1α by RNAi not only reduced the basal level of Ero1α but also abolished the increase of Ero1α expression induced by Hcy treatment (Fig. 3E). We surveyed the 5′ promoter region of the human *ERO1A* gene and found two putative hypoxia-response elements, HRE1 (-191/-184 nt) and HRE2 (-4079/-4072 nt), which exactly match the HIF-1 binding motif (5′-NCGTG-3′) (Fig. 3F). Chromatin immunoprecipitation (ChIP) assays performed in HUVECs showed that HRE1 but not HRE2 was enriched in HIF-1α immunoprecipitates after Hcy treatment (Fig. 3F). Taken together, these results show that Hcy upregulates Ero1α expression *via* promoting the binding of HIF-1α to HRE1 of the *ERO1A* promoter in endothelial cells.

2.4. Hcy activates Ero1α by perturbing ER redox balance in HUVECs

The sulfhydryl oxidase activity of Ero1α plays an important role in ER redox homeostasis maintenance. In the resting state, Ero1α predominantly exists in the inactive form and can be activated if the allosteric disulfides are reduced. To study whether Hcy leads to H_2O_2 production by activating Ero1α, we first monitored the redox states of Ero1α in HUVECs. As shown in Fig. 4A, cellular Ero1α shifted from the inactive Ox2 state to the active Ox1 state as early as 10 min after 200 μM Hcy treatment. As we previously reported that the activation of Ero1α was facilitated by reduced PDI, which was further dependent on the GSH/GSSG ratio [25], we next examined the effect of Hcy on the redox state of glutathione in the ER by using the ER-localized ratiometric fluorescent probe $roGFP_{ER}$ (Fig. S3A). The oxidizing agent diamide at 0.5 mM increased the ratio of fluorescence at 390/465 nm excitation, and the reducing agent DTT at 10 mM decreased the fluorescence ratio, validating the utility of the $roGFP_{ER}$ probe to monitor ER redox microenvironment in HUVECs (Figs. 4B and S3B). Notably, 200 μM Hcy caused a continuous decrease in the 390/465 nm

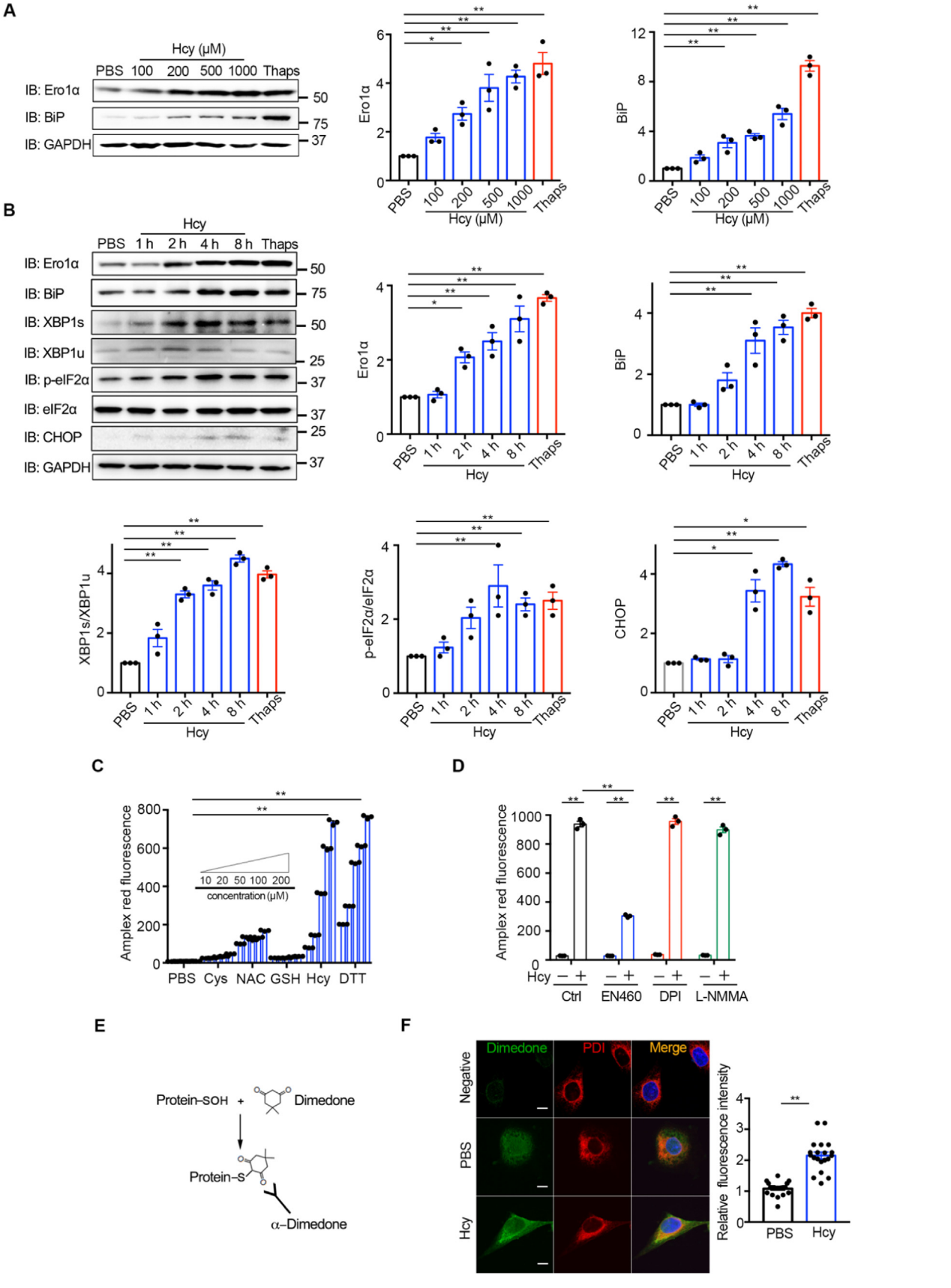

(caption on next page)

Fig. 2. Hcy upregulates Ero1α and induces ER stress and H_2O_2 accumulation in HUVECs. (A) HUVECs were treated without or with different concentrations of Hcy or 5 μM Thaps for 12 h. Cell lysates were subjected to immunoblotting and statistical analysis for Ero1α and BiP expression. Representative blots were shown. (B) HUVECs were treated with 200 μM Hcy for a different time as indicated or with 5 μM Thaps for 8 h. Cell lysates were subjected to immunoblotting and statistical analysis for expression of Ero1α, BiP, XBP1s/XBP1u, p-eIF2α/eIF2α, and CHOP. Representative blots were shown. (A-B) Data were shown as mean ± SEM from three independent experiments, *p < 0.05 and **p < 0.01 *via* one-way ANOVA, Tukey's multiple comparisons test. (C) HUVECs were pre-treated with indicated reducing agents at different concentrations of thiols for 1 h, and H_2O_2 levels were measured using Amplex red hydrogen peroxide/peroxidase assay. (D) HUVECs pre-treated with PBS, EN460 (100 μM), DPI (10 μM), and L-NMMA (1 mM) for 2 h were incubated in 200 μM Hcy for 1 h, and H_2O_2 levels were measured as in (C). (C–D) Data were shown as mean ± SEM from three independent experiments, *p < 0.05 and **p < 0.01 *via* two-way ANOVA, Tukey's multiple comparisons test. (E) Schematic diagram of detection of protein sulfenylation with an α-dimedone antibody. (F) HUVECs pre-treated with PBS or 200 μM Hcy for 4 h were incubated in media containing 5 mM dimedone for 1 h at 37 °C. Sulfenylated proteins (green, Ex = 488 nm) and the ER marker PDI (red, Ex = 568 nm) were analyzed by immunofluorescence. Nuclei were counterstained with Hoechst stain (blue, Ex = 405 nm). Scale bars, 10 μm. The relative fluorescence intensities from dimedone signals were quantified. Data were represented as mean ± SEM, N = 20 cells, **p < 0.01 *via* two-tailed Student's *t*-test.

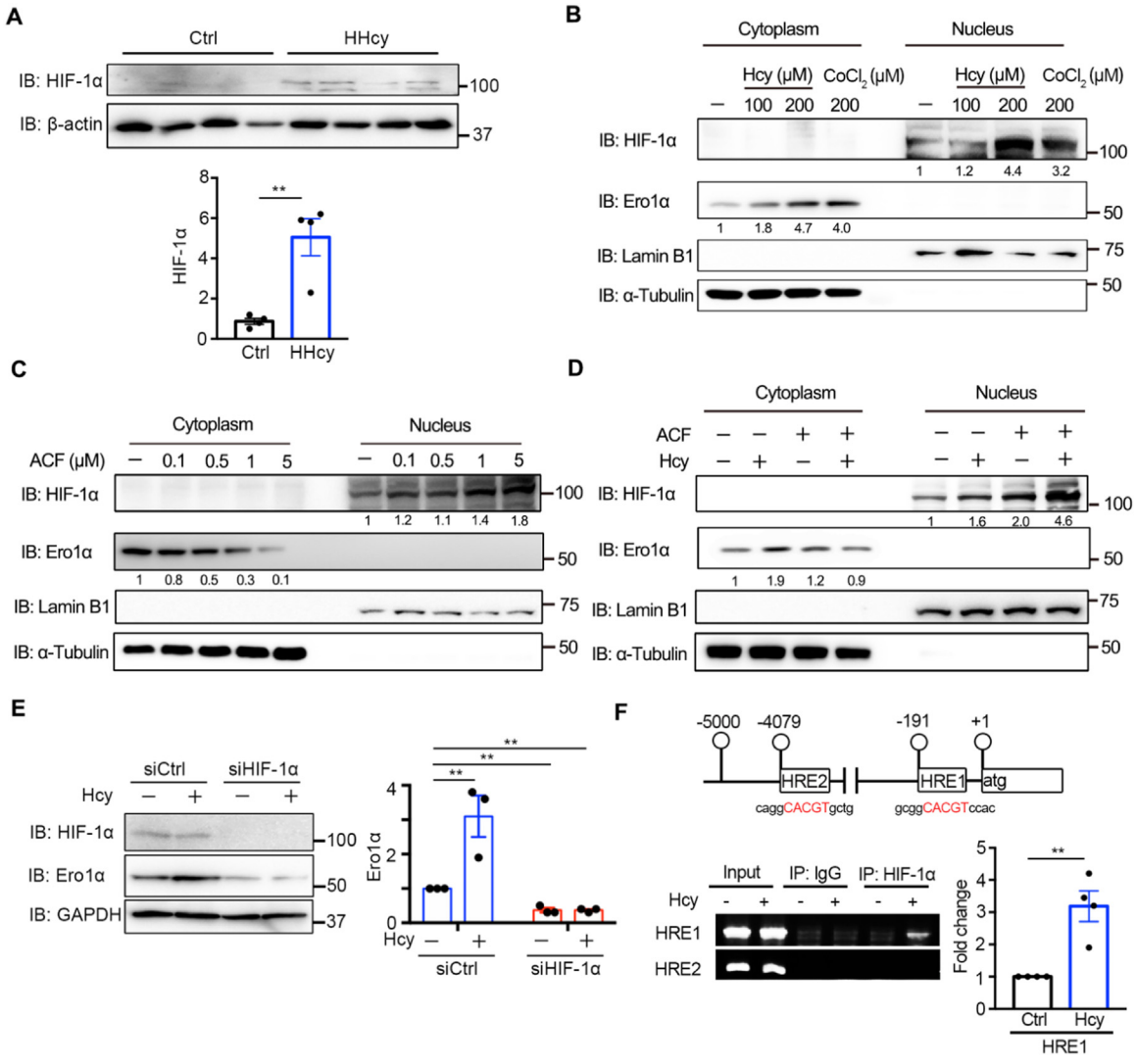

Fig. 3. Hcy-induced expression of Ero1α is through HIF-1α. (A) Lysates prepared from the thoracic aortas of normal (Ctrl) or HHcy mice were subjected to immunoblotting and statistical analysis for HIF-1α. Data were presented as mean ± SEM from four biological replicates, **p < 0.01 *via* two-tailed Student's *t*-test. (B) HUVECs were treated with indicated concentrations of Hcy or $CoCl_2$ for 4 h. Cytosolic Ero1α and nuclear HIF-1α were measured by immunoblotting with α-Tubulin and Lamin B1 as loading controls for cytosolic and nuclear extracts, respectively. (C) HUVECs were treated with different concentrations of ACF for 48 h, and immunoblotting was carried out as in (B). (D) HUVECs were pre-treated without or with 5 μM ACF for 1 h, then treated without or with 200 μM Hcy for an additional 4 h, and immunoblotting was carried out as in (B). (B–D) The relative density of each band was quantified as indicated below, which were representative results from two independent experiments. (E) HUVECs transfected with scrambled siRNA (siCtrl) or siRNA targeting HIF-1α for 72 h were treated with PBS or Hcy for 4 h. Cell lysates were analyzed by immunoblotting and statistical analysis for Ero1α. Data were shown as mean ± SEM from three independent experiments, **p < 0.01 *via* two-way ANOVA, Tukey's multiple comparisons test. (F) *(Upper)* Locations of the putative HRE-containing sites within the *ERO1A* promoter. The sequences that fit the consensus HRE motif were shown in red. *(Lower)* ChIP analysis of HIF-1α occupancy on the *ERO1A* promoter was performed with IgG or anti-HIF-1α antibody in HUVECs with or without 200 μM Hcy treatment for 4 h. The putative HRE1 and HRE2 were amplified by PCR and agarose gel electrophoresis. Enrichment values were shown as fold changes normalized to input. Data were presented as mean ± SEM from three independent experiments, **p < 0.01 *via* two-tailed Student's *t*-test.

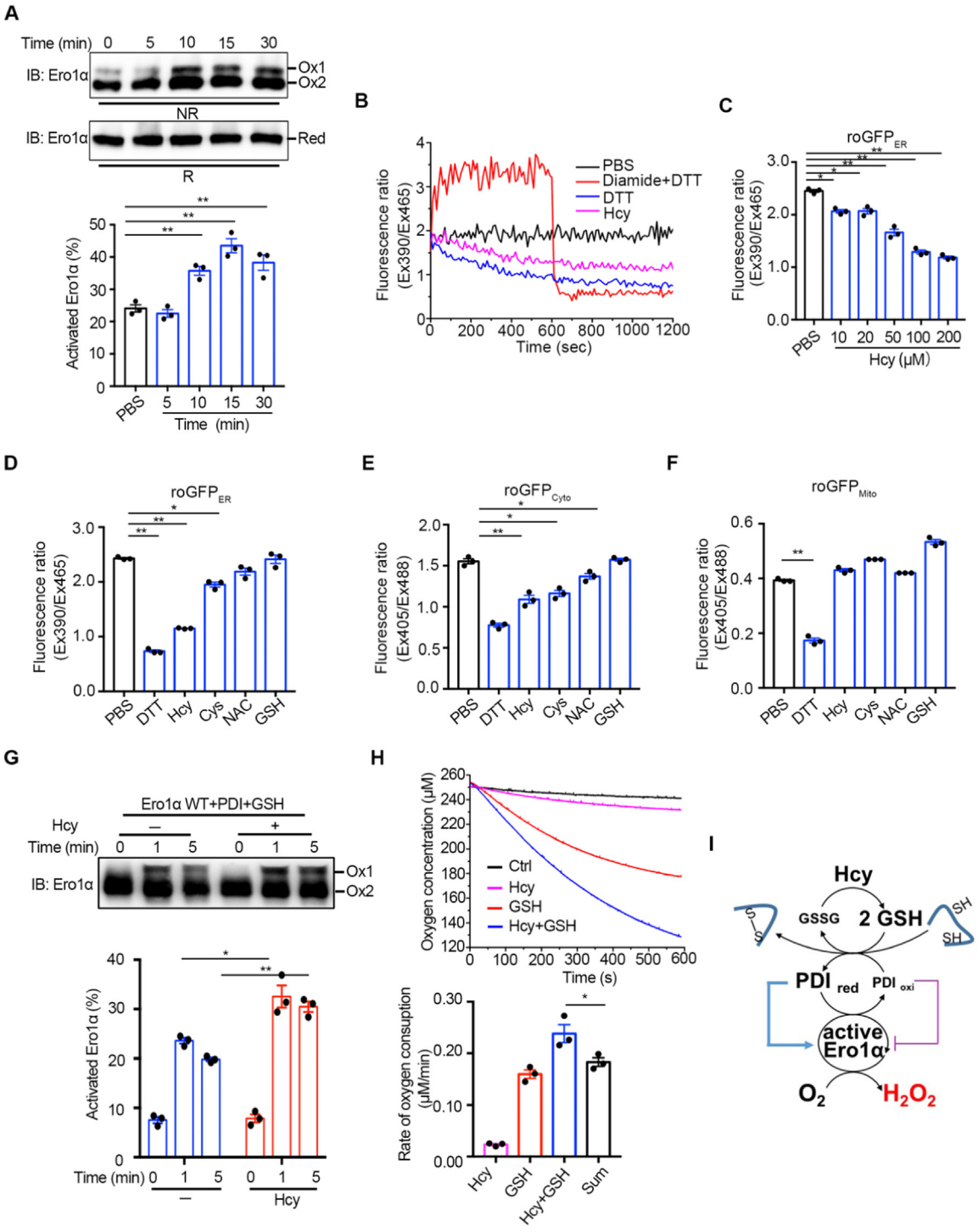

(caption on next page)

fluorescence ratio in HUVECs, similar to the effect of 100 μM DTT, suggesting that the GSH/GSSG ratio was increased in the ER lumen upon Hcy treatment. Moreover, Hcy as low as 50 μM can significantly reduce the ER redox state (Fig. 4C), and this effect caused by Hcy was prominent compared with other thiol agents (Fig. 4D). We also measured the effects of different thiol reagents on the redox states of cytosol and mitochondria by roGFP$_{Cyto}$ (Fig. S3C and D) and roGFP$_{Mito}$ (Fig. S3E and F), respectively. Compared to the ER redox change, there was less change in cytosolic redox state (Fig. 4E) and little change in mitochondria redox state (Fig. 4F) upon Hcy treatment.

The effects of Hcy on the Ero1α/PDI system mediated by GSH/GSSG were further confirmed *in vitro* by using recombinant proteins. In the absence of GSH, Hcy efficiently activated Ero1α only at the extremely high concentration of 10 mM (Fig. S4A). However, a fraction of Ero1α was immediately activated after incubation with PDI and GSH, and the addition of 200 μM Hcy into this system further promoted the activation of Ero1α (Figs. 4G and S4B). Since activated Ero1α can utilize oxygen to oxidize GSH through PDI, we thus monitored the oxygen consumption rate by using an oxygen electrode. Although Hcy was not an efficient substrate of Ero1α, its presence dramatically increased the rate of oxygen consumption catalyzed by Ero1α upon the oxidation of GSH (Fig. 4H). Moreover, overexpression of hyperactive Ero1α (C104/131A)

Fig. 4. Hcy activates Ero1α by reducing the redox states in the ER of HUVECs. (A) *(Upper)* HUVECs were treated with 200 μM Hcy and quenched with 20 mM NEM at indicated times. The cell lysates were analyzed by nonreducing (NR) or reducing (R) SDS-PAGE, followed by immunoblotting. Two oxidized Ero1α species (Ox1, active form; Ox2, inactive form) and fully reduced Ero1α (Red) were indicated. Representative blots were shown. (*Lower*) The ratio of activated Ero1α was quantified by densitometry and calculated. (B) HUVECs expressing $roGFP_{ER}$ were suspended in HBSS buffer (black) and treated with 0.5 mM diamide for 600 s, followed by the addition of 10 mM DTT (red), 100 μM DTT (blue), or 200 μM Hcy (pink). The ratio of fluorescence intensity was traced. (C) Measurement of $roGFP_{ER}$ fluorescence in HUVECs treated by PBS or different concentrations of Hcy for 30 min. (D–F) HUVECs transfected with $roGFP_{ER}$ (D) $roGFP_{Cyto}$ (E), or $roGFP_{Mito}$ (F) for 48 h were resuspended in HBSS buffer before treated with PBS or different reducing agents at 200 μM thiols as indicated for 30 min and then the fluorescence intensity ratio was detected. (A, C-F) Data were shown as mean ± SEM from three independent experiments, *$p < 0.05$ and **$p < 0.01$ *via* one-way ANOVA, Tukey's multiple comparisons test. (G) (*Upper*) Ero1α protein at 1 μM was incubated with 10 μM PDI protein and 1 mM glutathione in the presence or absence of 200 μM Hcy for a different time as indicated, and then analyzed by nonreducing SDS-PAGE and immunoblotting. Representative blots were shown. (*Lower*) The ratio of activated Ero1α were quantified as in (A). Data were shown as mean ± SEM from three independent experiments, *$p < 0.05$ and **$p < 0.01$ *via* two-way ANOVA, Tukey's multiple comparisons test. (H) (*Upper*) Oxygen consumption catalyzed by 2 μM Ero1α was monitored in the presence of 20 μM PDI without (black) or with 400 μM Hcy (pink), 2 mM GSH (red) or 400 μM Hcy plus 2 mM GSH (blue). (*Lower*) The slopes of the linear phases of oxygen decrease were taken as the oxygen consumption rates. The oxygen consumption rate in the control group (black) was taken as background and was subtracted in each group. The sum of the oxygen consumption rates in the presence of 400 μM Hcy or 2 mM GSH alone was taken as 'Sum'. Data were shown as mean ± SEM from three independent experiments, *$p < 0.05$ and **$p < 0.01$ *via* one-way ANOVA, Tukey's multiple comparisons test. (I) Schematic model illustrating that Hcy increases GSH/GSSG in the ER, therefore activates Ero1α and leads to H_2O_2 production.

rather than inactive Ero1α (C99/104A) resulted in the activation of the UPR signaling, further confirming that Ero1α activity is linked to ER stress (Fig. S5). Therefore, these results show that, although Hcy cannot be directly oxidized by the Ero1α/PDI system, it increases the GSH/GSSG ratio in the ER, which, in turn, activates Ero1α to produce more H_2O_2 and contributes to ER oxidative stress (Fig. 4I).

2.5. Ero1α knockdown ameliorates HHcy-induced ER oxidative stress and inflammation in endothelium

Hcy not only promoted Ero1α expression but also increased its oxidase activity. Next, we asked whether Hcy-induced ER oxidative stress could be ameliorated by Ero1α depletion. As shown in Fig. 5A, Ero1α knockdown in HUVECs was successfully achieved by using lentiviral shRNA vectors and markedly inhibited Hcy-induced BiP expression. Specifically, activation of the IRE1 and PERK pathways by Hcy treatment was greatly attenuated. Ero1α deficiency also attenuated Hcy-induced upregulation of the adhesion molecules ICAM-1 and VCAM-1. In addition, Ero1α depletion largely prevented the release of H_2O_2 from HUVECs (Fig. 5B) and the Hcy-induced accumulation of ER-localized sulfenylated proteins (Fig. 5C). More importantly, knockdown of Ero1α, both in the cultured aortic rings *ex vivo* (Figs. 5D and S6A–C) and in the carotid arteries of HHcy mice *in vivo* (Figs. 5E and S6D–F), led to downregulation of ICAM-1 and BiP under HHcy condition. These results indicate that depletion of Ero1α has a protective effect against Hcy-induced ER oxidative stress and vascular endothelial inflammation.

2.6. The NRF2-GPx7 axis is activated by acute Hcy treatment in HUVECs

Ero1α-produced H_2O_2 must be promptly eliminated to avoid ROS accumulation and ER over-oxidation. We also investigated whether Hcy affects the expression of ER antioxidants. So far, three peroxidase enzymes (peroxiredoxin Prx4, glutathione peroxidase GPx7 and GPx8) have been reported to localize in the ER lumen. After 200 μM Hcy treatment for 8 h, the mRNA levels of *ERO1A* and *GPX7* were significantly upregulated, whereas *PRX4* and *GPX8* were not induced (Fig. 6A). GPx7 is responsible for direct elimination of the H_2O_2 produced by Ero1α [30]. We have previously elucidated that GPx7 can be induced in human fibroblasts by NRF2, the master transcription factor responsible for cellular antioxidant response [32]. Here, we observed that the protein expression of NRF2 and GPx7 in HUVECs was elevated time-dependently after Hcy treatment (Fig. 6B). Immunofluorescence analysis showed that nuclear accumulation of NRF2 was promoted by Hcy, albeit less efficiently than by the NRF2 activator tertiary butyl hydroquinone (tBHQ) (Fig. 6C). Then we found that Hcy activated NRF2 through oxidation of Kelch-like ECH-associated protein 1 (Keap1), a component of Cullin-3-type ubiquitin ligase for NRF2 (Figure S7). This phenomenon was reminiscent of H_2O_2 treatment [48], implying that Hcy administration resulted in H_2O_2 accumulation. Moreover, the basal level of GPx7 decreased in *NRF2* knockdown HUVECs, and Hcy-induced upregulation of GPx7 was largely abolished when NRF2 was depleted (Fig. 6D). Therefore, after acute Hcy treatment in HUVECs, ER-localized peroxidase GPx7 is upregulated through transcriptional activation of NRF2, probably in order to cope with ER oxidative stress.

2.7. GPx7 protects against endothelial dysfunction caused by Hcy-induced ER oxidative stress

To our surprise, the protein levels of NRF2 and GPx7 in the thoracic aortas of chronic HHcy mice greatly declined (Fig. 7A), which contrasted with the results of acute Hcy stimulation *in vitro*. By contrast, the levels of Prx4 and GPx8 were not changed (Fig. S8). Immunofluorescence staining also showed that the intensity of GPx7 was decreased during HHcy treatment (Fig. 7B). In HUVECs, the expression of GPx7 was induced by Hcy within 24 h and later suppressed up to 72 h, while Ero1α was continuously upregulated (Fig. S9). We therefore speculated that the inactivation of the NRF2-GPx7 pathway may aggravate Hcy-induced ER oxidative stress in the vascular system. As confirmation of the protective role of GPx7 under the condition of HHcy, HA-tagged GPx7 with ER localization (Fig. S10) was overexpressed in HUVECs using lentiviral vectors before Hcy treatment. Ectopic expression of GPx7 markedly alleviated Hcy-induced ER stress as indicated by BiP and p-eIF2α immunoblotting (Fig. 7C). Moreover, overexpression of GPx7 inhibited the production of H_2O_2 upon Hcy treatment (Fig. 7D) and attenuated ER-localized sulfenylated protein accumulation (Fig. 7E). In line with this, overexpression of GPx7 prevented Hcy-induced upregulation of ICAM-1 and BiP in cultured aortic rings *ex vivo* (Figs. 7F and S11A, B) and in the carotid arteries of HHcy mice *in vivo* (Figs. 7G and S11C). Taken together, these results suggest that GPx7 protects endothelial cells from Hcy-induced ER oxidative stress and that its deficiency may contribute to HHcy-induced vasculopathy.

3. Discussion

HHcy has been demonstrated to cause endothelial dysfunction through cellular oxidative stress and ER stress. In this work, we provide the first evidence that redox homeostasis in the ER is the link between the oxidative stress and ER stress under Hcy treatment. The ER sulfhydryl oxidase Ero1α is responsible for ER over-oxidation and ER stress, both in Hcy-treated endothelium and in a chronic HHcy mouse model. At the transcriptional level, Hcy promotes the binding of HIF-1α to the HRE of the *ERO1A* promoter then upregulates Ero1α expression. At the post-translational level, Hcy allosterically activates Ero1α by increasing the GSH/GSSG ratio and reduced PDI level in the ER. The increased

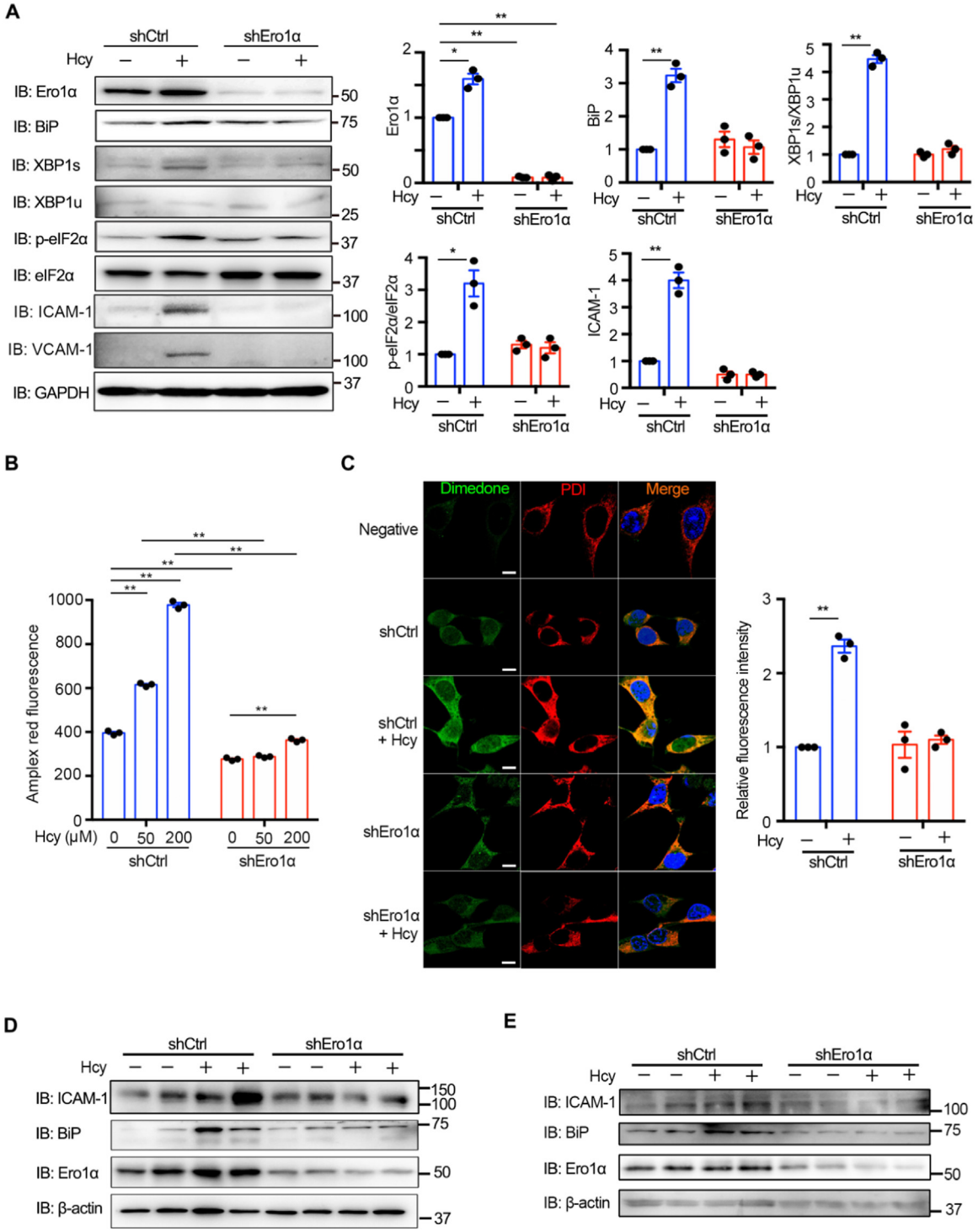

Fig. 5. Knockdown of Ero1α ameliorates Hcy-induced ER oxidative stress in endothelium. (A) HUVECs transduced with lentiviral control shRNA (shCtrl) or shEro1α for more than 72 h were treated with 200 μM Hcy for an additional 4 h. The protein levels of Ero1α, BiP, XBP1s/XBP1u, p-eIF2α/eIF2α, ICAM-1, and VCAM-1 were determined by immunoblotting and statistical analysis. Representative blots were shown. (B) HUVECs transduced with lentiviral shCtrl or shEro1α for more than 72 h were treated without or with different concentrations of Hcy for 1 h, and H_2O_2 levels were measured as in Fig. 2C. (C) HUVECs transduced with lentiviral shCtrl or shEro1α were treated without or with 200 μM Hcy for 4 h. Sulfenylated proteins (green, Ex = 568 nm) and the ER marker PDI (red, Ex = 647 nm) were analyzed by immunofluorescence. Nuclei were counterstained with Hoechst stain (blue, Ex = 405 nm). Scale bars, 20 μm. The relative fluorescence intensities from dimedone signals were quantified. (A–C) Data were represented as mean ± SEM from three independent experiments, *p < 0.05 and **p < 0.01 *via* two-way ANOVA, Tukey's multiple comparisons test. (D) *Ex vivo* aortic ring assays. Mouse thoracic aortas were transduced with adenovirus vector expressing shCtrl or shEro1α for 48 h, followed by treatment without or with 200 μM Hcy for 4 h and immunoblotting analysis. Representative blots were shown. The statistical analysis of ICAM-1, BiP, and Ero1α expression was shown in Fig. S6A–C. (E) *In vivo* external carotid artery injection assays were performed as described in Methods. Mice were locally injected in the external carotid arteries with adenovirus vector expressing shCtrl or shEro1α for 72 h, then injected with saline or Hcy through the tail vein. After 1 h the carotid arteries were harvested for immunoblotting analysis. Representative blots were shown. The statistical analysis of ICAM-1, BiP, and Ero1α expression was shown in Fig. S6D–F.

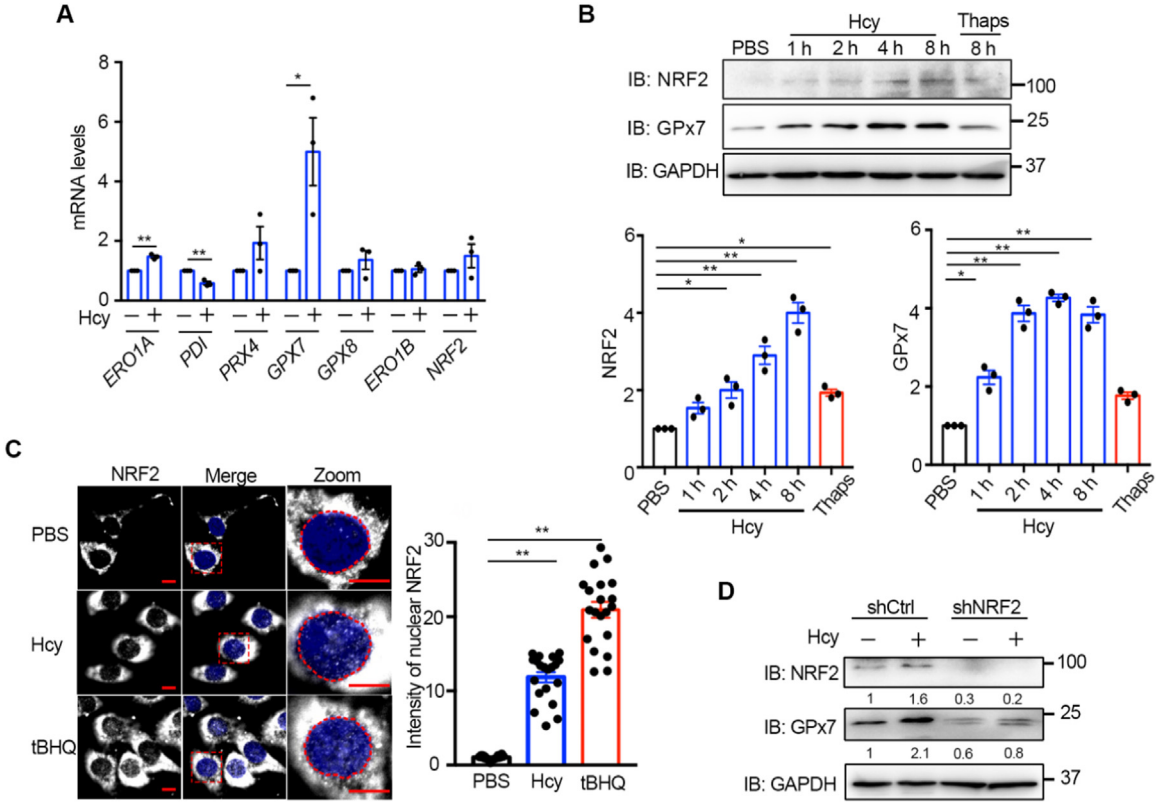

Fig. 6. Hcy activates the NRF-2/GPx7 pathway in HUVECs. (A) RT-qPCR analysis of ER redox-related genes in HUVECs treated without or with 200 μM Hcy for 8 h. All values were normalized to β-ACTIN mRNA. Data were represented as mean ± SEM from three independent experiments each performed in three technical replicates, *p < 0.05 and **p < 0.01 *via* two-tailed Student's *t*-test. (B) HUVECs were treated with 200 μM Hcy for different times as indicated or with 5 μM Thaps for 8 h. The cell lysates were subjected to immunoblotting and statistical analysis for NRF2 and GPx7 expression. Representative blots were shown. Data were represented as mean ± SEM from three independent experiments. *p < 0.05 and **p < 0.01 *via* one-way ANOVA, Tukey's multiple comparisons test. (C) Immunofluorescence analysis of the translocation of NRF2 (Ex = 488 nm) into the nucleus (blue, Ex = 405 nm) in HUVECs treated with 200 μM Hcy or 200 μM tertiary butyl hydroquinone (tBHQ) or PBS for 2 h. The nuclei were outlined with red circles. Scale bars, 10 μm. The relative fluorescence intensities from nuclear-localized NRF2 were quantified. Data were represented as mean ± SEM, N = 20 cells, **p < 0.01 *via* one-way ANOVA, Tukey's multiple comparisons test. (D) HUVECs transduced with lentiviral shCtrl or shNRF2 for more than 72 h were treated without or with 200 μM Hcy for 4 h. The protein levels of NRF2 and GPx7 were determined by immunoblotting and quantified by densitometry as indicated below, which were representative results from two independent experiments.

Ero1α activity produces excess H_2O_2 and leads to protein over-oxidation in the ER, activation of UPR pathways and endothelial inflammation. On the other hand, the ER antioxidant pathway mediated by GPx7 is impaired during HHcy, further emphasizing the importance of the balance between Ero1α and GPx7 in HHcy-induced vasculopathy (Fig. 8).

Notably, by using redox-sensitive GFP targeted in different cellular compartment, we observe that at pathophysiological concentration Hcy markedly reduces the ER redox state by increasing the GSH/GSSG ratio, but has less effect on the redox state of mitochondrial and cytosol. This is likely because that the ER is much more oxidizing than other cellular compartment [49], and is more sensitive to a reductive stress. Moreover, the effects on ER redox state and H_2O_2 release caused by Hcy are much more significant than those caused by other thiol agents, underlining the specific role of Hcy. Importantly, we find that Ero1α acts as a redox control switch that immediately changes the reducing power of Hcy into the oxidizing power of H_2O_2. To our knowledge, this is the first evidence that Hcy as a reducing agent, by elevating GSH/GSSG level, can trigger oxidative stress in the ER. The accumulation of H_2O_2 causes over-oxidation of ER proteins, which leads to the activation of UPR, inflammatory, and even antioxidant pathways.

In line with our observation, recent studies showed that expression of a hyperactive mutant form of Ero1α causes UPR activation [49] and that ROS could enhance IRE1 and PERK signaling by promoting oxidation of UPR sensors or of PDIs [50]. Moreover, Ero1α is involved in ER calcium influx and efflux. Ero1α inhibits SERCA Ca^{2+} pump activity [51] and stimulates IP_3R-dependent Ca^{2+} flux to the cytosol and mitochondria [52,53]. Ca^{2+} flux across the ER-mitochondria contact sites stimulates mitochondrial outer membrane permeabilization and respiratory chain dysfunction, leading to an increase in ROS, which further enhances Ca^{2+} release and causes fatal UPR and apoptosis [54,55]. Indeed, mice lacking ERO1α are partially protected against progressive heart failure in a transaortic constriction model [56]. Additionally, knockdown of Ero1α ameliorates HHcy-induced ER oxidative stress and inflammation in HUVECs and in mice (Fig. 5).

We also find that the Ero1α-GPx7 axis plays a critical role in ER redox homeostasis regulation during HHcy. The ER resident peroxidases GPx7 is elevated under accurate Hcy stimulation, which is consistent with the previous finding that GPx7 [30] and its homologue GPx8 [57] are crucial for the control of Ero1α-derived ROS diffusion. In this model, the Ero1α/GPx7/PDI triad utilizes a single O_2 molecule to generate two disulfide bonds and two harmless H_2O molecules (Fig. 8) [30]. We further identify that GPx7 upregulation is dependent on the antioxidant transcription factor NRF2. Interestingly, it has been reported that the NRF2 antioxidant response can be activated by IRE1 [58] and PERK [59] signaling. Thus, Ero1α-H_2O_2-IRE1/PERK-NRF2-GPx7 may constitute a feedback loop that governs ER redox homeostasis and prevents endothelial inflammation and dysfunction under acute Hcy stress (Fig. 8). Notably, the expression of GPx7 in the thoracic aorta of chronic HHcy mice is largely suppressed. GPx7 deficiency therefore results in ER redox imbalance and accounts for Hcy-induced vasculopathy. The question that remains unanswered is how GPx7 is

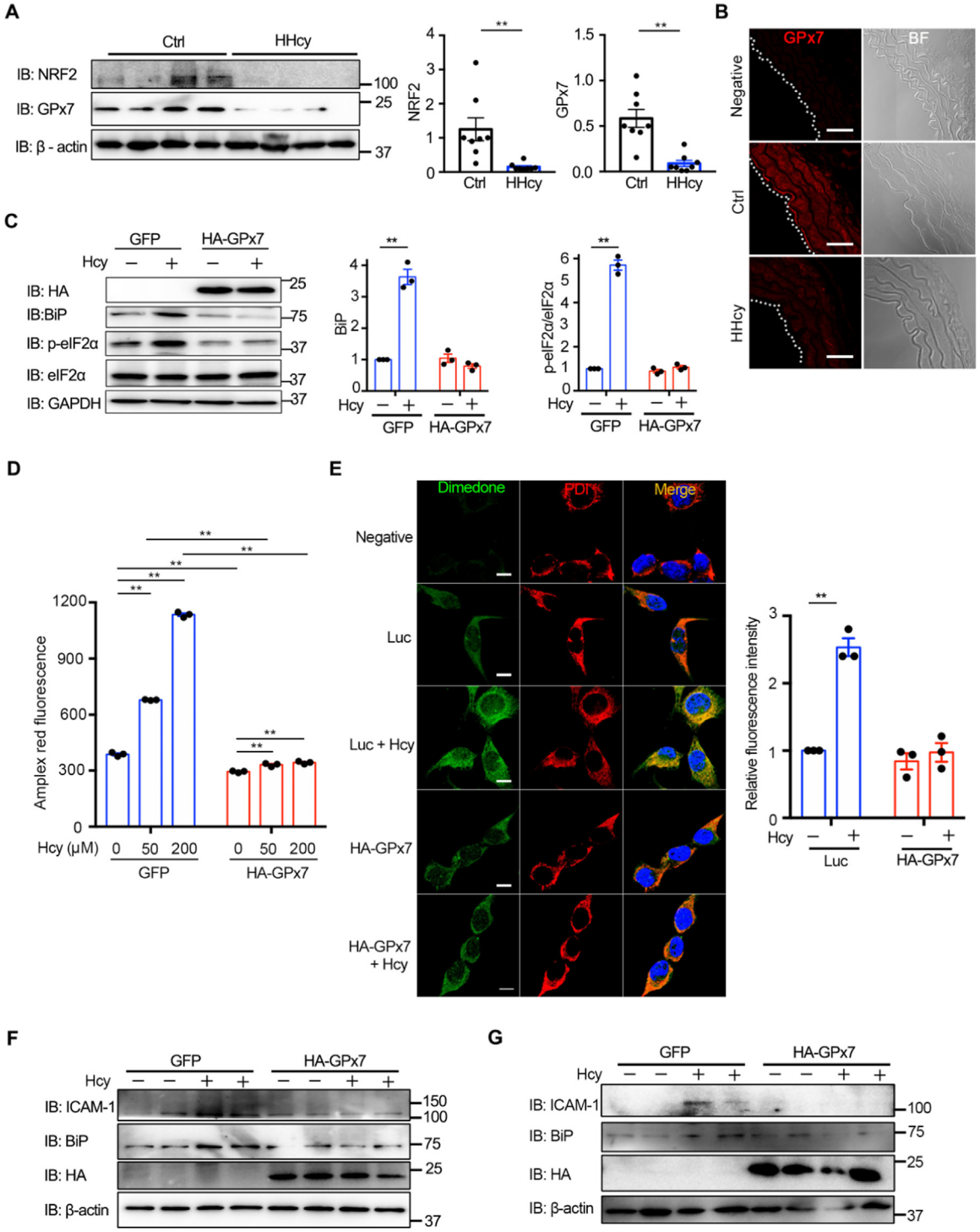

Fig. 7. GPx7 protects endothelium against Hcy-induced ER oxidative stress. (A) Lysates prepared from the thoracic aortas of normal (Ctrl) or HHcy mice were subjected to immunoblotting and statistical analysis for NRF2 and GPx7 expression. Representative blots were shown. Data were represented as mean ± SEM from eight biological replicates, *p < 0.05 *via* two-tailed Student's *t*-test. (B) Immunofluorescence analysis of GPx7 (red, Ex = 568 nm) from the thoracic aortas of Ctrl and HHcy mice with rabbit IgG as a negative control. The aortic intima is indicated by white dashed line. BF, bright field. Scale bars, 50 μm. (C) HUVECs transduced with lentivirus expressing GFP or HA-tagged GPx7 (HA-GPx7) for more than 72 h were treated without or with 200 μM Hcy for 4 h and subjected to immunoblotting. The expression of BiP and p-eIF2α/eIF2α was analyzed. Representative blots were shown. (D) HUVECs lentivirus expressing GFP or HA-tagged GPx7 (HA-GPx7) for more than 72 h were treated without or with different concentration of Hcy for 1 h, and H_2O_2 levels were measured as in Fig. 2C. (E) HUVECs transduced with lentiviral luciferase (Luc) or HA-GPx7 were treated without or with 200 μM Hcy for 4 h. Cells were analyzed by immunofluorescence as in Fig. 5C. Scale bars, 20 μm. The relative fluorescence intensities from dimedone signals were quantified. (C–E) Data were represented as mean ± SEM from three independent experiments, **p < 0.01 *via* two-way ANOVA, Tukey's multiple comparisons test. (F) *Ex vivo* aortic ring assays. Mouse thoracic aortas were transduced with adenovirus vector expressing GFP or HA-GPx7 for 48 h, followed by treatment without or with 200 μM Hcy for 4 h and immunoblotting analysis. Representative blots were shown. The statistical analysis of ICAM-1 and BiP was shown in Fig. S11A, B. (G) *In vivo* external carotid artery injection assays with adenovirus vector expressing GFP or HA-GPx7 were carried out as in Fig. 5E. Representative blots were shown. The statistical analysis of BiP was shown in Fig. S11C.

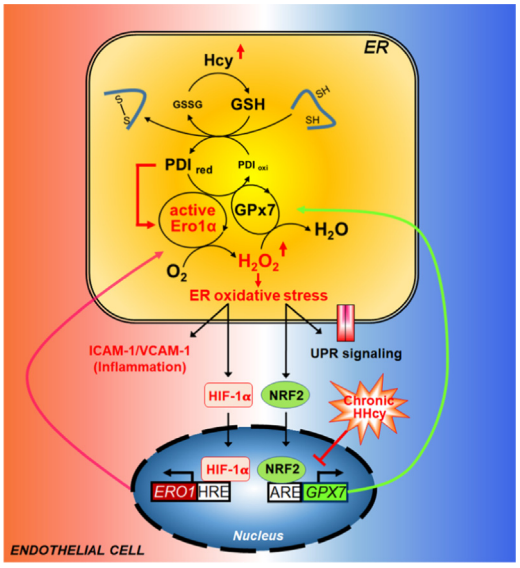

Fig. 8. A working model illustrating HHcy-induced ER oxidative stress and inflammation in endothelial cells. At steady state, the Ero1α/GPx7/PDI triad safeguards ER redox homeostasis during oxidative protein folding. In this scenario, O_2 is consumed by Ero1α to produce H_2O_2, which is further utilized by GPx7, with H_2O being released. An elevated Hcy level increases the GSH/GSSG ratio in the ER of endothelial cells, which, in turn, generates additional reduced PDI (PDI_{red}) from oxidized PDI (PDI_{oxi}). Reduced PDI quickly activates Ero1α, leading to the accumulation of H_2O_2, which results in ER over-oxidation. On one hand, ER oxidative stress can cause inflammatory activation by upregulating the expression of ICAM-1/VCAM-1 adhesion molecules and HIF-1α. HIF-1α positively regulates the expression of Ero1α and may further amplify H_2O_2 accumulation and oxidative stress. On the other hand, over-oxidation of ER can also activate UPR signaling and elicit a cellular antioxidant response through NRF2. In particular, NRF2 induces GPx7 expression to scavenge Ero1α-produced H_2O_2 and to re-establish ER redox homeostasis. However, in chronic HHcy pathology, the NRF2-GPx7 antioxidant pathway is restrained in endothelial cells, which exaggerates ER oxidative stress and further contributes to endothelial inflammation and vasculopathy.

silenced in chronic HHcy. One possible explanation is that Hcy can be metabolized to methionine; the latter can rapidly form *S*-adenosyl methionine, which is a methyl donor for DNA and RNA methylation [35,60], and GPx7 can be silenced by promoter DNA hypermethylation [61]. Therefore, in endothelial tissue under the stress of HHcy, the decrease in GPx7, in addition to the increase in Ero1α, further exaggerates ER redox disorders and contributes to HHcy-induced vasculopathy.

Taken together, our results highlight the importance of ER oxidative stress in HHcy-induced vascular endothelial inflammation and shed light on the possibility of targeting ER redox homeostasis as an intervention for endothelial dysfunction-related vascular diseases, including arteriosclerosis, hypertension, stroke, and ischemia/reperfusion damage.

4. Materials and methods

4.1. Reagents and antibodies

Homocysteine (Hcy), thapsigargin (Thaps), acriflavine (ACF), tertiary butyl hydroquinone (tBHQ), diamide, glutathione (GSH), dithiothreitol (DTT), N-ethylmaleimide (NEM), N-acetylcysteine (NAC), L-cysteine (Cys), diphenylene iodonium (DPI), and Hoechst stain were purchased from Sigma-Aldrich. N^G-Monomethyl-L-arginine monoacetate salt (L-NMMA, Abcam) and EN460 (Merck Millipore). The following antibodies were used in this work: anti-GPx7 (Abclonal, A3902), anti-NRF2 (Abcam, ab62352), anti-BiP (Sigma, G8918), anti-Ero1α (Merck Millipore, MABT376), anti-XBP1 (Santa Cruz, sc-7160), anti-p-eIF2α (Cell Signaling Technology, D9G8), anti-eIF2α (Abclonal, D7D3), anti-CHOP (Cell Signaling Technology, L63F7), anti-GAPDH (Sigma-Aldrich, G9295), anti-β-actin (Sigma-Aldrich, A3854), anti-ICAM-1 (Santa Cruz, sc-7891), anti-VCAM-1 (Santa Cruz, sc-8304), anti-α-tubulin (Sigma-Aldrich, T6074), anti-Lamin B1 (Abcam, ab16048), anti-HIF-1α (Novusbio, NB100-105), anti-dimedone (Merck Millipore, ABS30), anti-calreticulin (Abcam, ab2907), anti-PDI (Abcam, ab2792), non-specific mouse IgG (Beyotime, A7028), goat anti-rabbit IgG-peroxidase (Sigma-Aldrich, A0545), goat anti-mouse IgG-peroxidase (Sigma-Aldrich, A4416), goat anti-rabbit Alexa Fluor 488 (Invitrogen, A11034), goat anti-mouse Alexa Fluor 568 (Invitrogen, A11004), goat anti-rabbit Alexa Fluor 568 (Invitrogen, A21069), and goat anti-mouse Alexa Fluor 647 (Invitrogen, A31571).

4.2. HHcy mouse model and cell culture

For the chronic HHcy model, male C57BL/6J mice (6–8 w), purchased from the Animal Center of Peking University Health Science Center, were maintained with or without 1.8 g/l DL-Hcy in their drinking water for 4 w. The mice were randomly divided into different treated groups. The total plasma Hcy was quantified to be 20–30 μM by gas chromatography-mass spectrometry as we described before [62]. For the acute HHcy model, mice were injected with Hcy (50 mg/kg dissolved in 0.4 ml normal saline) through tail vein. Human umbilical vein endothelial cells (HUVECs, from Dr. X. Yan, Institute of Biophysics, CAS) [63] and HEK293T cells (from Dr. G. H. Liu, Institute of Biophysics, CAS) were cultured in RPMI 1640 media (HyClone) supplemented with 10% fetal bovine serum (Gibco) and penicillin/streptomycin (Gibco). All cells were cultured at 37 °C in a humidified atmosphere containing 5% CO_2. For knocking down HIF-1α, HUVECs were transfected with siRNA targeting *HIF1A* (sense: UACUCAGAGCU UUGGAUCAAGUUAA and anti-sense: UUAACUUGAUCCAAAGCUCUG AGUA) or a scrambled stealth RNAi duplex (Invitrogen) for 72 h using RNAi MAX (Invitrogen).

4.3. Lentivirus preparation

The cDNA of HA-tagged GPx7 (HA-GPx7), HA-tagged Ero1α or its mutants, FLAG-luciferase and GFP were cloned into a pLE4 lentiviral vector kindly provided by Dr. G. H. Liu (Institute of Biophysics, CAS). shRNA sequences targeting human *ERO1A* (GGGCTTTATCCAAAGTGT TACCATT) and *NRF2* (GTAAGAAGCCAGATGTTAA) were cloned into pLVTHM/GFP (Addgene, 12247). Lentivirus particles were generated from HEK293T cells by co-transfecting lentiviral vectors with the packaging plasmids psPAX2 (Addgene) and pMD2G (Addgene), for transduction in the presence of 4 μg/ml polybrene.

4.4. Ex vivo aortic ring assay

Ex vivo aortic ring assays were carried out as previously described [64]. Briefly, C57BL/6 male mice (6–8 w) were sacrificed by CO_2 inhalation. The isolated thoracic aortas were washed with serum-free RPMI 1640 media, cleaned of connective tissue, and divided into 1–2 mm rings, that were then cultured with endothelial cell basal medium (Lonza, CC-3156) supplemented with 10% fetal bovine serum (Gibco). Adenovirus vectors (Hanbio Biotechnology) expressing a control shRNA or an shRNA targeting mouse *ERO1A* (CAGCTCTTCACTG GGAATAAA), GFP or HA-GPx7 cDNA were transduced into the cultured aortic rings, which were then cultured for 48–72 h. Phosphate-buffered saline (PBS) or 200 μM Hcy was added, and after 4 h the aortic rings were lysed, followed by immunoblotting analysis.

4.5. In vivo external carotid artery injection assay

In vivo external carotid artery injection assay was performed

according to the protocol reported [65,66] with some modifications. Male C57BL/6J mice (6–8 w) were first applied with a U-clip on the bottom of the left carotid artery and the left internal carotid artery, and the external carotid artery was ligated with stitches. 0.1 ml of adenovirus vector expressing a control shRNA or an shRNA targeting mouse *ERO1A*, GFP or HA-GPx7 cDNA (1×10^{10} TU/ml) was injected to the lumen of the external carotid arteries with a needle. 40 min later, the clip was loosed and the skin was sutured. After 72 h, normal saline (0.4 ml) or Hcy (50 mg/kg dissolved in 0.4 ml normal saline) was injected into the tail vein. In this model, the plasma level of Hcy can reach up to 1000 μM in 5 min after administration, and remains at 50 μM at 90 min [67]. The mice were sacrificed by CO_2 inhalation 1 h after injection, and the carotid arteries were harvested, lysed, and subjected to immunoblotting analysis. The carotid arteries were prepared by a professional technician and the immunoblotting were analyzed by another investigator, both of whom were blinded to the assessment of the analyses.

4.6. Nuclear/cytosol fractionation

HUVECs were lysed with cytoplasmic lysis buffer (10 mM HEPES buffer, pH 7.9, 1.5 mM $MgCl_2$, 10 mM KCl, 0.4% (v/v) NP-40, 1 mM DTT, and protease inhibitor cocktail), and the lysates were collected by centrifugation at 12,000*g* for 3 min. The intact nuclei were washed twice with cytoplasmic lysis buffer and then lysed in nuclear lysis buffer (20 mM HEPES buffer, pH 7.9, 0.1 mM EGTA, 0.2 mM EDTA, 420 mM NaCl, 1 mM DTT, 25% (v/v) glycerol, 0.1% (v/v) NP-40, and protease inhibitor cocktail) with vortex for 30 min at 4 °C. The nucleoplasmic fraction was collected by centrifugation at 12,000*g* for 15 min.

4.7. Immunoblotting assay

HUVECs or thoracic aorta were lysed in lysis buffer (Merck Millipore) with protease inhibitor cocktail (Roche) and phosphatase inhibitor cocktail (Roche). Protein concentrations were quantified using a BCA Kit (Beyotime). Portions of lysate with equal amount of protein were subjected to SDS-PAGE and then electrotransferred to a polyvinylidene fluoride membrane (Merck Millipore). After being blocked with 10% bovine serum albumin (BSA), the membrane was incubated with primary antibodies (1:1000 or 1:500) overnight at 4 °C, followed by incubation with peroxidase-conjugated goat anti-rabbit or anti-mouse IgG (1:5000) for 1 h at room temperature, and then detected by enhanced chemiluminescence (Thermo Scientific) and imaged using a ChemiScope Mini chemiluminescence imaging system (Clinx Science). Band intensities were quantified using the software ImageJ (National Institutes of Health).

4.8. Immunofluorescence staining assay

HUVECs and thoracic aortas were fixed with acetone-methanol (1:1, v/v) for 15 min at − 20 °C, washed in PBS, and blocked with 10% BSA in PBS with 0.1% Triton X-100 (PBST) for 30 min. HUVECs were incubated with anti-NRF2 (1:200), and the frozen thoracic aorta sections were incubated with anti-Ero1α (1:200) and anti-ICAM-1 (1:100) overnight at 4 °C, then washed with PBST and incubated with goat anti-rabbit Alexa Fluor 488 (1:500)/goat-anti-mouse Alexa Fluor 568 (1:500) for 1 h. The cells were counterstained with 0.05 mg/ml Hoechst stain for 10 min, rinsed with Hank's Balanced Salt Solution (HBSS, Gibco), and analyzed by confocal laser scanning microscopy (Zeiss, LSM710).

4.9. Protein sulfenylation determination

HUVECs pre-treated with Hcy for 4 h were incubated with 5 mM dimedone for 1 h at 37 °C, washed with PBS and fixed with acetone-methanol (1:1, v/v) for 10 min at − 20 °C, then washed again with PBS. After being blocked with 10% BSA in PBST for 30 min at room temperature, the cells were incubated with anti-dimedone (1:2000) and anti-PDI (1:1000) in PBST overnight at 4 °C. After being washed with PBST, the cells were incubated with goat anti-rabbit Alexa Fluor 488 (1:500)/goat anti-mouse Alexa Fluor 568 (1:500) or goat anti-rabbit Alexa Fluor 568 (1:500)/goat anti-mouse Alexa Fluor 647 (1:500) in PBST for 1 h, washed with HBSS, counterstained with 0.05 mg/ml Hoechst for 10 min, and rinsed with HBSS. Finally, the cells were analyzed by confocal laser scanning microscopy (Zeiss, LSM710).

4.10. Reverse transcription quantitative PCR (RT-qPCR)

RNA of 2 μg prepared using TRIzol Reagent (Invitrogen) was reverse transcribed into cDNA with a GoScript Reverse Transcription System (Promega). qPCR was carried out using SYBR Select Master Mix (Applied Biosystems) and a QuantStudio 7 Flex machine (Applied Biosystems), following the manufacturer's instructions. All qPCR primer pairs were listed in Table S1, and the relative mRNA levels were normalized to *β-ACTIN* and calculated as $2^{-\Delta\Delta CT}$.

4.11. Chromatin immunoprecipitation (ChIP) assay

ChIP assays were performed as previously described [68]. Briefly, HUVECs were treated with Hcy or PBS for 2 h, then cross-linked by 1% formaldehyde. The cells were then lysed. The released chromatin was sonicated for being sheared into fragments. HIF-1α protein was immunoprecipitated by mouse anti-HIF-1α monoclonal antibody or non-specific mouse IgG. After protease K digestion, the de-crosslinked DNA was extracted for PCR analysis with primers flanking the putative hypoxia response element (HRE) within the *ERO1A* promoter. The products were resolved by 1.5% agarose gel electrophoresis. All the primers are listed in Table S2.

4.12. Determination of H_2O_2

The production of cellular H_2O_2 was quantified by using the a Amplex red hydrogen peroxide/peroxidase assay kit (Invitrogen, A22188). HUVECs (100,000 cells) were harvested, resuspended in HBSS, seeded into a 96-well plate and cultured with different reducing agents for 1 h at 37 °C. 50 μM Amplex red reagent and 0.1 U/ml horseradish peroxidase (HRP) in HBSS was added into each well and incubated at room temperature for 30 min. The fluorescence intensity at 590 nm with excitation at 545 nm was traced using a Varioskan Flash (Thermo Fisher).

4.13. ER redox state examination

The plasmid expressing an ER-localized redox-sensitive green fluorescent protein (roGFP1-iE_{ER}) [69] was a generous gift from Dr. C. Appenzeller-Herzog (University of Basel), and additional mutations (S30R, T39N, N105T, I171V) were inserted to generate superfolded-roGFP-iE_{ER} (hereafter referred to as $roGFP_{ER}$) as described [70]. The plasmid expressing mitochondria-localized Grx1-roGFP2 (hereafter referred to as $roGFP_{mito}$) was kindly provided by Dr. T. P. Dick (Heidelberg University), and cytosolic Grx1-roGFP2 (hereafter referred to as $roGFP_{cyto}$) was kindly provided by Dr. C. Chen (Institute of Biophysics, CAS). For the redox state measurement, HUVECs were transfected with $roGFP_{ER}$, $roGFP_{mito}$, or $roGFP_{cyto}$ using Lipofectamine 2000 (Invitrogen). After 48 h, cells were trypsinized, washed by HBSS, and seeded in a 96-well plate. After addition of oxidizing or reducing agents, time-dependent fluorescence changes of $roGFP_{ER}$ at 515 nm were traced with excitation at 390 and 465 nm using a Varioskan Flash (Thermo Fisher). The fluorescence changes of $roGFP_{mito}$ or $roGFP_{cyto}$ were recorded at 525 nm with excitation at 405 and 488 nm.

4.14. Ero1α redox state measurement in cells

HUVECs were treated with Hcy for different times, immediately blocked with 20 mM NEM for 15 min, and then lysed using lysis buffer (Merck Millipore) containing 50 mM NEM. The lysates were analyzed by nonreducing SDS-9%PAGE and immunoblotting to determine the redox states of Ero1α. Two oxidized Ero1α species (Ox1, active form; Ox2, inactive form) and fully reduced Ero1α (Red) were indicated. The ratio of activated Ero1α was quantified by densitometry and calculated as (Ox1/(Ox1 + Ox2) × 100%).

4.15. Ero1α redox state determination in vitro

Ero1α and PDI proteins were purified as previously described [25]. A mixture of 200 μM Hcy, 10 μM PDI protein and 1 mM GSH was pre-incubated in reaction buffer (50 mM Tris-HCl, pH 7.6, 150 mM NaCl, 2 mM EDTA) at 25 °C for 30 min. The reaction was started by adding Ero1α protein to a final concentration of 1 μM. Aliquots were taken at different times, quenched with 20 mM NEM, and analyzed by non-reducing SDS-9%PAGE followed by immunoblotting to determine the redox states of Ero1α.

4.16. Oxygen consumption assay in vitro

Oxygen consumption was measured at 25 °C using an Oxygraph Clark-type oxygen electrode (Hansatech Instruments) as described previously [25]. Briefly, reactions were initiated by adding Ero1α protein to a final concentration of 2 μM in oxygen consumption buffer (100 mM Tris-HAc, pH 8.0, 50 mM NaCl, 2 mM EDTA, 20 μM PDI protein) containing 2 mM GSH or 400 μM Hcy.

4.17. Statistical analysis

The number of independent experiments/biological replicates/technical replicates used for comparison was indicated in each figure legend. Data was expressed as mean ± SEM. The two-tailed Student's *t*-test was used to analyze data between two groups and the ANOVA followed by Tukey's multiple comparisons test were used when more than two groups were present. Statistical significance was considered when $p < 0.05$. Significance levels were defined as $*p < 0.05$; $**p < 0.01$.

4.18. Ethics statement

All mouse husbandry and experiments were carried out in accordance with the Guide for the Care and Use of Laboratory Animals of the Health Science Center of Peking University, and all efforts were made to minimize the animals' suffering.

Acknowledgements

We are grateful to Guang-Hui Liu for the kind gift of the pLVTHM-shNRF2 plasmid; to Xiyun Yan for the present of HUVECs; to Tobias P. Dick for the kind gift of the plasmid expressing mitochondria-localized Grx1-roGFP2; to Chang Chen for the plasmid expressing cytosolic Grx1-roGFP2 and to Lulu Sun for providing blood vessel of chronic HHcy mice, Xi Wang and Changtao Jiang for helpful discussion. This work was supported by the National Key R&D Program of China (2017YFA0504000, 2016YFA0500200); the National Natural Science Foundation of China (31771261, 31571163, 81770445, 91439206); and the Youth Innovation Promotion Association, CAS, to LW.

Author contributions

X.WU, X.WANG, C.C.W., J.F., and L.W. designed the research. X.WU, L.Z., Y.M., and J.Y. performed the experiments. X.WU, J.F., and L.W. analyzed the data. X.WU, J.F. and L.W. with contributions from X.WANG and C.C.W. wrote the manuscript.

Conflict of interest

The authors declare no competing interests.

Appendix A. Supplementary material

Supplementary data associated with this article can be found in the online version at doi:10.1016/j.redox.2018.09.021.

References

[1] K.S. McCully, Vascular pathology of homocysteinemia: implications for the pathogenesis of arteriosclerosis, Am. J. Pathol. 56 (1969) 111–128.
[2] R. Clarke, L. Daly, K. Robinson, E. Naughten, S. Cahalane, B. Fowler, I. Graham, Hyperhomocysteinemia: an independent risk factor for vascular disease, N. Engl. J. Med. 324 (1991) 1149–1155.
[3] K. Robinson, A. Gupta, V. Dennis, K. Arheart, D. Chaudhary, R. Green, P. Vigo, E.L. Mayer, J. Selhub, M. Kutner, D.W. Jacobsen, Hyperhomocysteinemia confers an independent increased risk of atherosclerosis in end-stage renal disease and is closely linked to plasma folate and pyridoxine concentrations, Circulation 94 (1996) 2743–2748.
[4] R.T. Eberhardt, M.A. Forgione, A. Cap, J.A. Leopold, M.A. Rudd, M. Trolliet, S. Heydrick, R. Stark, E.S. Klings, N.I. Moldovan, M. Yaghoubi, P.J. Goldschmidt-Clermont, H.W. Farber, R. Cohen, J. Loscalzo, Endothelial dysfunction in a murine model of mild hyperhomocyst(e)inemia, J. Clin. Invest. 106 (2000) 483–491.
[5] A.F. Perna, D. Ingrosso, N.G. De Santo, Homocysteine and oxidative stress, Amino Acids 25 (2003) 409–417.
[6] D. Zhang, X. Xie, Y. Chen, B.D. Hammock, W. Kong, Y. Zhu, Homocysteine upregulates soluble epoxide hydrolase in vascular endothelium in vitro and in vivo, Circ. Res. 110 (2012) 808–817.
[7] R.C. Austin, S.R. Lentz, G.H. Werstuck, Role of hyperhomocysteinemia in endothelial dysfunction and atherothrombotic disease, Cell Death Differ. 11 (Suppl. 1) (2004) S56–S64.
[8] J. Zhou, G.H. Werstuck, S. Lhotak, A.B. de Koning, S.K. Sood, G.S. Hossain, J. Moller, M. Ritskes-Hoitinga, E. Falk, S. Dayal, S.R. Lentz, R.C. Austin, Association of multiple cellular stress pathways with accelerated atherosclerosis in hyperhomocysteinemic apolipoprotein E-deficient mice, Circulation 110 (2004) 207–213.
[9] Q. Zhang, X. Zeng, J. Guo, X. Wang, Effects of homocysteine on murine splenic B lymphocyte proliferation and its signal transduction mechanism, Cardiovasc. Res. 52 (2001) 328–336.
[10] Y. Taniyama, K.K. Griendling, Reactive oxygen species in the vasculature: molecular and cellular mechanisms, Hypertension 42 (2003) 1075–1081.
[11] J.A. Sipkens, N. Hahn, C.S. van den Brand, C. Meischl, S.A. Cillessen, D.E. Smith, L.J. Juffermans, R.J. Musters, D. Roos, C. Jakobs, H.J. Blom, Y.M. Smulders, P.A. Krijnen, C.D. Stehouwer, J.A. Rauwerda, V.W. van Hinsbergh, H.W. Niessen, Homocysteine-induced apoptosis in endothelial cells coincides with nuclear NOX2 and peri-nuclear NOX4 activity, Cell Biochem. Biophys. 67 (2013) 341–352.
[12] L. Jin, R.B. Caldwell, T. Li-Masters, R.W. Caldwell, Homocysteine induces endothelial dysfunction via inhibition of arginine transport, J. Physiol. Pharmacol. 58 (2007) 191–206.
[13] V. Bermudez, F. Bermudez, G. Acosta, A. Acosta, J. Anez, C. Andara, E. Leal, C. Cano, V. Manuel, R. Hernandez, Z. Israili, Molecular mechanisms of endothelial dysfunction: from nitric oxide synthesis to ADMA inhibition, Am. J. Ther. 15 (2008) 326–333.
[14] R. Zhou, A.S. Yazdi, P. Menu, J. Tschopp, A role for mitochondria in NLRP3 inflammasome activation, Nature 469 (2011) 221–225.
[15] E. Szegezdi, S.E. Logue, A.M. Gorman, A. Samali, Mediators of endoplasmic reticulum stress-induced apoptosis, EMBO Rep. 7 (2006) 880–885.
[16] L. Wang, X. Wang, C.C. Wang, Protein disulfide-isomerase, a folding catalyst and a redox-regulated chaperone, Free Radic. Biol. Med. 83 (2015) 305–313.
[17] B.P. Tu, J.S. Weissman, Oxidative protein folding in eukaryotes: mechanisms and consequences, J. Cell Biol. 164 (2004) 341–346.
[18] A. Mezghrani, A. Fassio, A. Benham, T. Simmen, I. Braakman, R. Sitia, Manipulation of oxidative protein folding and PDI redox state in mammalian cells, EMBO J. 20 (2001) 6288–6296.
[19] A.M. Benham, A. Cabibbo, A. Fassio, N. Bulleid, R. Sitia, I. Braakman, The CXXCXXC motif determines the folding, structure and stability of human Ero1-Lalpha, EMBO J. 19 (2000) 4493–4502.
[20] Y.H. Seo, K.S. Carroll, Profiling protein thiol oxidation in tumor cells using sulfenic acid-specific antibodies, Proc. Natl. Acad. Sci. USA 106 (2009) 16163–16168.
[21] J. Han, S.H. Back, J. Hur, Y.H. Lin, R. Gildersleeve, J. Shan, C.L. Yuan, D. Krokowski, S. Wang, M. Hatzoglou, M.S. Kilberg, M.A. Sartor, R.J. Kaufman, ER-stress-induced transcriptional regulation increases protein synthesis leading to cell death, Nat. Cell Biol. 15 (2013) 481–490.
[22] J.E. Chambers, S.J. Marciniak, Cellular mechanisms of endoplasmic reticulum stress signaling in health and disease. 2. Protein misfolding and ER stress, Am. J. Physiol. Cell Physiol. 307 (2014) C657–C670.
[23] C.S. Sevier, H. Qu, N. Heldman, E. Gross, D. Fass, C.A. Kaiser, Modulation of cellular

disulfide-bond formation and the ER redox environment by feedback regulation of Ero1, Cell 129 (2007) 333–344.
[24] S. Kim, D.P. Sideris, C.S. Sevier, C.A. Kaiser, Balanced Ero1 activation and inactivation establishes ER redox homeostasis, J. Cell Biol. 196 (2012) 713–725.
[25] L. Zhang, Y. Niu, L. Zhu, J. Fang, X. Wang, L. Wang, C.C. Wang, Different interaction modes for protein-disulfide isomerase (PDI) as an efficient regulator and a specific substrate of endoplasmic reticulum oxidoreductin-1alpha (Ero1alpha), J. Biol. Chem. 289 (2014) 31188–31199.
[26] D.M. Battle, S.D. Gunasekara, G.R. Watson, E.M. Ahmed, C.G. Saysell, N. Altaf, A.L. Sanusi, P.C. Munipalle, D. Scoones, J. Walker, Y. Viswanath, A.M. Benham, Expression of the endoplasmic reticulum oxidoreductase Ero1alpha in gastro-intestinal cancer reveals a link between homocysteine and oxidative protein folding, Antioxid. Redox Signal. 19 (2013) 24–35.
[27] R. Brigelius-Flohe, M. Maiorino, Glutathione peroxidases, Biochim. Biophys. Acta 2013 (1830) 3289–3303.
[28] V.D. Nguyen, M.J. Saaranen, A.R. Karala, A.K. Lappi, L. Wang, I.B. Raykhel, H.I. Alanen, K.E. Salo, C.C. Wang, L.W. Ruddock, Two endoplasmic reticulum PDI peroxidases increase the efficiency of the use of peroxide during disulfide bond formation, J. Mol. Biol. 406 (2011) 503–515.
[29] N. Weiss, Y.Y. Zhang, S. Heydrick, C. Bierl, J. Loscalzo, Overexpression of cellular glutathione peroxidase rescues homocyst(e)ine-induced endothelial dysfunction, Proc. Natl. Acad. Sci. USA 98 (2001) 12503–12508.
[30] L. Wang, L. Zhang, Y. Niu, R. Sitia, C.C. Wang, Glutathione peroxidase 7 utilizes hydrogen peroxide generated by Ero1alpha to promote oxidative protein folding, Antioxid. Redox Signal. 20 (2014) 545–556.
[31] P.C. Wei, Y.H. Hsieh, M.I. Su, X. Jiang, P.H. Hsu, W.T. Lo, J.Y. Weng, Y.M. Jeng, J.M. Wang, P.L. Chen, Y.C. Chang, K.F. Lee, M.D. Tsai, J.Y. Shew, W.H. Lee, Loss of the oxidative stress sensor NPGPx compromises GRP78 chaperone activity and induces systemic disease, Mol. Cell 48 (2012) 747–759.
[32] J. Fang, J. Yang, X. Wu, G. Zhang, T. Li, X. Wang, H. Zhang, C.C. Wang, G.H. Liu, L. Wang, Metformin alleviates human cellular aging by upregulating the endoplasmic reticulum glutathione peroxidase 7, Aging Cell (2018) e12765.
[33] Y. Li, C. Jiang, G. Xu, N. Wang, Y. Zhu, C. Tang, X. Wang, Homocysteine upregulates resistin production from adipocytes in vivo and in vitro, Diabetes 57 (2008) 817–827.
[34] R.P. Schleimer, B.S. Bochner, Endothelial leukocyte adhesion molecule-1 and intercellular adhesion molecule-1 mediate the adhesion of eosinophils to endothelial cells in vitro and are expressed by endothelium in allergic cutaneous inflammation in vivo, J. Immunol. 147 (1991) 380–381.
[35] Y.H. Luo, J. Feng, Q.B. Xu, W.G. Wang, X. Wang, NSun2 deficiency protects endothelium from inflammation via mRNA methylation of ICAM-1, Circ. Res. 118 (2016) 944–956.
[36] D. May, A. Itin, O. Gal, H. Kalinski, E. Feinstein, E. Keshet, Ero1-L alpha plays a key role in a HIF-1-mediated pathway to improve disulfide bond formation and VEGF secretion under hypoxia: implication for cancer, Oncogene 24 (2005) 1011–1020.
[37] K.S. Woo, P. Chook, Y.I. Lolin, A.S. Cheung, L.T. Chan, Y.Y. Sun, J.E. Sanderson, C. Metreweli, D.S. Celermajer, Hyperhomocyst(e)inemia is a risk factor for arterial endothelial dysfunction in humans, Circulation 96 (1997) 2542–2544.
[38] J.C. Chambers, P.M. Ueland, M. Wright, C.J. Dore, H. Refsum, J.S. Kooner, Investigation of relationship between reduced, oxidized, and protein-bound homocysteine and vascular endothelial function in healthy human subjects, Circ. Res. 89 (2001) 187–192.
[39] S.H. Mudd, J.D. Finkelstein, H. Refsum, P.M. Ueland, M.R. Malinow, S.R. Lentz, D.W. Jacobsen, L. Brattstrom, B. Wilcken, D.E. Wilcken, H.J. Blom, S.P. Stabler, R.H. Allen, J. Selhub, I.H. Rosenberg, Homocysteine and its disulfide derivatives: a suggested consensus terminology, Arterioscler. Thromb. Vasc. Biol. 20 (2000) 1704–1706.
[40] T. Li, B. Yu, Z. Liu, J. Li, M. Ma, Y. Wang, M. Zhu, H. Yin, X. Wang, Y. Fu, F. Yu, X. Wang, X. Fang, J. Sun, W. Kong, Homocysteine directly interacts and activates the angiotensin II type I receptor to aggravate vascular injury, Nat. Commun. 9 (2018) 11.
[41] H. Xi, Y. Zhang, Y. Xu, W.Y. Yang, X. Jiang, X. Sha, X. Cheng, J. Wang, X. Qin, J. Yu, Y. Ji, X. Yang, H. Wang, Caspase-1 inflammasome activation mediates homocysteine-induced pyrop-apoptosis in endothelial cells, Circ. Res. 118 (2016) 1525–1539.
[42] V. Mishin, J.P. Gray, D.E. Heck, D.L. Laskin, J.D. Laskin, Application of the Amplex red/horseradish peroxidase assay to measure hydrogen peroxide generation by recombinant microsomal enzymes, Free Radic. Biol. Med. 48 (2010) 1485–1491.
[43] C. Branco-Price, N. Zhang, M. Schnelle, C. Evans, D.M. Katschinski, D. Liao, L. Ellies, R.S. Johnson, Endothelial cell HIF-1alpha and HIF-2alpha differentially regulate metastatic success, Cancer Cell 21 (2012) 52–65.
[44] T. Bishop, P.J. Ratcliffe, HIF hydroxylase pathways in cardiovascular physiology and medicine, Circ. Res. 117 (2015) 65–79.
[45] B. Gess, K.H. Hofbauer, R.H. Wenger, C. Lohaus, H.E. Meyer, A. Kurtz, The cellular oxygen tension regulates expression of the endoplasmic oxidoreductase ERO1-Lalpha, Eur. J. Biochem. 270 (2003) 2228–2235.
[46] C. Jiang, J.H. Kim, F. Li, A. Qu, O. Gavrilova, Y.M. Shah, F.J. Gonzalez, Hypoxia-inducible factor 1alpha regulates a SOCS3-STAT3-adiponectin signal transduction pathway in adipocytes, J. Biol. Chem. 288 (2013) 3844–3857.
[47] K. Lee, H. Zhang, D.Z. Qian, S. Rey, J.O. Liu, G.L. Semenza, Acriflavine inhibits HIF-1 dimerization, tumor growth, and vascularization, Proc. Natl. Acad. Sci. USA 106 (2009) 17910–17915.
[48] S. Fourquet, R. Guerois, D. Biard, M.B. Toledano, Activation of NRF2 by nitrosative agents and H_2O_2 involves KEAP1 disulfide formation, J. Biol. Chem. 285 (2010) 8463–8471.
[49] D.A. Hudson, S.A. Gannon, C. Thorpe, Oxidative protein folding: from thiol-disulfide exchange reactions to the redox poise of the endoplasmic reticulum, Free Radic. Biol. Med. 80 (2015) 171–182.
[50] D. Eletto, E. Chevet, Y. Argon, C. Appenzeller-Herzog, Redox controls UPR to control redox, J. Cell Sci. 127 (2014) 3649–3658.
[51] D. Di Marino, I. D'Annessa, A. Coletta, A. Via, A. Tramontano, Characterization of the differences in the cyclopiazonic acid binding mode to mammalian and P. Falciparum Ca^{2+} pumps: a computational study, Proteins 83 (2015) 564–574.
[52] G. Li, M. Mongillo, K.T. Chin, H. Harding, D. Ron, A.R. Marks, I. Tabas, Role of ERO1-alpha-mediated stimulation of inositol 1,4,5-triphosphate receptor activity in endoplasmic reticulum stress-induced apoptosis, J. Cell Biol. 186 (2009) 783–792.
[53] T. Anelli, L. Bergamelli, E. Margittai, A. Rimessi, C. Fagioli, A. Malgaroli, P. Pinton, M. Ripamonti, R. Rizzuto, R. Sitia, Ero1alpha regulates Ca(2+) fluxes at the endoplasmic reticulum-mitochondria interface (MAM), Antioxid. Redox Signal. 16 (2012) 1077–1087.
[54] A.P. Arruda, B.M. Pers, G. Parlakgul, E. Guney, K. Inouye, G.S. Hotamisligil, Chronic enrichment of hepatic endoplasmic reticulum-mitochondria contact leads to mitochondrial dysfunction in obesity, Nat. Med. 20 (2014) 1427–1435.
[55] J. Feng, S. Lu, Y. Ding, M. Zheng, X. Wang, Homocysteine activates T cells by enhancing endoplasmic reticulum-mitochondria coupling and increasing mitochondrial respiration, Protein Cell 7 (2016) 391–402.
[56] K.T. Chin, G. Kang, J. Qu, L.B. Gardner, W.A. Coetzee, E. Zito, G.I. Fishman, D. Ron, The sarcoplasmic reticulum luminal thiol oxidase ERO1 regulates cardiomyocyte excitation-coupled calcium release and response to hemodynamic load, FASEB J. 25 (2011) 2583–2591.
[57] T. Ramming, H.G. Hansen, K. Nagata, L. Ellgaard, C. Appenzeller-Herzog, GPx8 peroxidase prevents leakage of H2O2 from the endoplasmic reticulum, Free Radic. Biol. Med. 70 (2014) 106–116.
[58] J.M. Hourihan, L.E. Moronetti Mazzeo, L.P. Fernandez-Cardenas, T.K. Blackwell, Cysteine sulfenylation directs IRE-1 to activate the SKN-1/Nrf2 antioxidant response, Mol. Cell 63 (2016) 553–566.
[59] S.B. Cullinan, J.A. Diehl, PERK-dependent activation of Nrf2 contributes to redox homeostasis and cell survival following endoplasmic reticulum stress, J. Biol. Chem. 279 (2004) 20108–20117.
[60] P.R. Mandaviya, L. Stolk, S.G. Heil, Homocysteine and DNA methylation: a review of animal and human literature, Mol. Genet. Metab. 113 (2014) 243–252.
[61] D. Peng, T. Hu, M. Soutto, A. Belkhiri, A. Zaika, W. El-Rifai, Glutathione peroxidase 7 has potential tumour suppressor functions that are silenced by location-specific methylation in oesophageal adenocarcinoma, Gut 63 (2014) 540–551.
[62] Y. Li, H. Zhang, C. Jiang, M. Xu, Y. Pang, J. Feng, X. Xiang, W. Kong, G. Xu, Y. Li, X. Wang, Hyperhomocysteinemia promotes insulin resistance by inducing endoplasmic reticulum stress in adipose tissue, J. Biol. Chem. 288 (2013) 9583–9592.
[63] Y. Kang, F. Wang, J. Feng, D. Yang, X. Yang, X. Yan, Knockdown of CD146 reduces the migration and proliferation of human endothelial cells, Cell Res. 16 (2006) 313–318.
[64] G.R. Small, P.W. Hadoke, I. Sharif, A.R. Dover, D. Armour, C.J. Kenyon, G.A. Gray, B.R. Walker, Preventing local regeneration of glucocorticoids by 11beta-hydroxysteroid dehydrogenase type 1 enhances angiogenesis, Proc. Natl. Acad. Sci. USA 102 (2005) 12165–12170.
[65] D. Nam, C.W. Ni, A. Rezvan, J. Suo, K. Budzyn, A. Llanos, D.G. Harrison, D.P. Giddens, H. Jo, A model of disturbed flow-induced atherosclerosis in mouse carotid artery by partial ligation and a simple method of RNA isolation from carotid endothelium, J. Vis. Exp. 40 (2010) e1861.
[66] J. Zhou, P.L. Lee, C.I. Lee, S.Y. Wei, S.H. Lim, T.E. Lin, S. Chien, J.J. Chiu, BMP receptor-integrin interaction mediates responses of vascular endothelial Smad1/5 and proliferation to disturbed flow, J. Thromb. Haemost. 11 (2013) 741–755.
[67] H.P. Zhao, J. Feng, K. Sun, Y.Y. Liu, X.H. Wei, J.Y. Fan, P. Huang, X.W. Mao, Z. Zhou, C.S. Wang, X. Wang, J.Y. Han, Caffeic acid inhibits acute hyperhomocysteinemia-induced leukocyte rolling and adhesion in mouse cerebral venules, Microcirculation 19 (2012) 233–244.
[68] J.A. Dahl, P. Collas, A rapid micro chromatin immunoprecipitation assay (microChIP), Nat. Protoc. 3 (2008) 1032–1045.
[69] J. Birk, M. Meyer, I. Aller, H.G. Hansen, A. Odermatt, T.P. Dick, A.J. Meyer, C. Appenzeller-Herzog, Endoplasmic reticulum: reduced and oxidized glutathione revisited, J. Cell Sci. 126 (2013) 1604–1617.
[70] J. Hoseki, A. Oishi, T. Fujimura, Y. Sakai, Development of a stable ERroGFP variant suitable for monitoring redox dynamics in the ER, Biosci. Rep. 36 (2016) e00316.